Author/s:
Bienroth, D;Charitakis, N;Wong, D;Zhang, YC;Jaeger-Honz, S;Ding, J;Watt, KI;Stolper, J;Chambers-Smith, H;MacGregor, D;Christiansen, B;Vivien, C;Piers, AT;Waylen, LN;Hoffmann, LB;Tang, J;La, HM;Du, MRM;Mohenska, M;Polo, JM;Grimmond, S;Scott, E;Rossello, FJ;Porrello, ER;Klein, K;Nim, HT;Elliott, DA;Schreiber, F;Ramialison, M

Title:
Automated integration of multi-slice spatial transcriptomics data in 2D and 3D using VR-Omics

Date:
2025-12-01

Citation:
Bienroth, D., Charitakis, N., Wong, D., Zhang, Y. C., Jaeger-Honz, S., Ding, J., Watt, K. I., Stolper, J., Chambers-Smith, H., MacGregor, D., Christiansen, B., Vivien, C., Piers, A. T., Waylen, L. N., Hoffmann, L. B., Tang, J., La, H. M., Du, M. R. M., Mohenska, M. ,... Ramialison, M. (2025). Automated integration of multi-slice spatial transcriptomics data in 2D and 3D using VR-Omics. Genome Biology, 26 (1), pp.182-. https://doi.org/10.1186/s13059-025-03630-6.

Persistent Link:
https://hdl.handle.net/11343/362030

Genome Biology

METHODOLOGY

Open Access

Automated integration of multi-slice spatial transcriptomics data in 2D and 3D using VR-Omics

Denis Bienroth[1†], Natalie Charitakis[1,2†], Dillon Wong[1], Yunhan C. Zhang[1], Sabrina Jaeger-Honz[3], Jialin Ding[1], Kevin I. Watt[1,6], Julian Stolper[1,2], Hazel Chambers-Smith[4], Duncan MacGregor[4], Bronwyn Christiansen[4], Celine Vivien[1], Adam T. Piers[1,5], Lisa N. Waylen[1], Lucas B. Hoffmann[6], Jessica Tang[1], Hue M. La[7,8], Mei R. M. Du[1], Monika Mohenska[9,10,11], Jose M. Polo[9,10,11], Sean Grimmond[7], Ethan Scott[6], Fernando J. Rossello[1,12,13], Enzo R. Porrello[1,5,6†], Karsten Klein[3†], Hieu T. Nim[1,2,13†], David A. Elliott[1,2,13*†], Falk Schreiber[3,14*†] and Mirana Ramialison[1,2,13*†]

[†]Denis Bienroth and Natalie Charitakis are co-first authors.

[†]Enzo R. Porrello, Karsten Klein, Hieu T. Nim, David A. Elliott, Falk Schreiber and Mirana Ramialison are co-senior authors.

*Correspondence: David.Elliott@mcri.edu.au; Falk.Schreiber@uni-konstanz.de; Mirana.Ramialison@mcri.edu.au

[1] Novo Nordisk Foundation Center for Stem Cell Medicine, Murdoch Children's Research Institute, Parkville, VIC 3052, Australia
[3] Department of Computer and Information Science, University of Konstanz, Constance 78464, Germany
Full list of author information is available at the end of the article

Abstract

The field of spatial transcriptomics is rapidly evolving, with increasing sample complexity, resolution, and tissue size. Yet the field lacks comprehensive and intuitive solutions for automated integration and analysis of multi-slice data in either co-planar (2D) or stacked (3D) formation. To address this, we develop VR-Omics, a free, platform-agnostic software that provides end-to-end automated processing of multi-slice data through a biologist-friendly interface. Benchmarking against existing methods demonstrates VR-Omics' unique strengths to perform comprehensive end-to-end analysis of multi-slice stacked data. Through co-planar slice analysis, VR-Omics uncovers previously undetected, dysregulated metabolic networks within rare pediatric cardiac rhabdomyomas, demonstrating its potential for biological discoveries.

Background

Spatial transcriptomics (ST) is a ground-breaking technology allowing the capture of spatial gene expression at unprecedented resolution to advance our comprehension of cellular processes and molecular mechanisms [1–3]. Capitalising on the potential of ST approaches, the size of tissue samples being profiled often exceeds a standard vendor-provided chip size, necessitating the generation of multi-slice datasets. Those datasets are typically either co-planar, where adjacent slices within the same anatomical plane to form a continuous composite (e.g., twelve prostate cryosections sections [4]) or three-dimensional (3D) stacked, consisting of consecutive parallel slices where sequential sections preserve spatial continuity along the tissue depth (e.g., thirteen E16.5 mouse embryo sections [5]). Facilitating multi-slice data analysis enables tissues to be studied

in their complete native spatial context, providing crucial insights, and understanding of the tissue structure and characteristics.

Several ST algorithms have been developed to process and mine ST multi-slice data, including Stitch3D [6] and VT3D [7]. However, these specialised multi-slice pipelines and analytical programs have limited functionality within the scope of an end-to-end analysis pipeline of ST data while also requiring advanced computational skills, creating a substantial barrier for end-users. Several online portals allow visualisation of existing multi-slice ST datasets (SpatialDB [8], STOmicsDB [9], SODB [10], SOAR [11]) but limit the user to the datasets that are publicly available and do not allow the analysis of user-uploaded multi-slice data. Finally, there is a lack of ST tools that allow manual interactive alignment and downstream processing of multi-slice data (both co-planar and 3D stacked formations), by providing an interactive graphical user interface (GUI).

Here we present VR-Omics, an interactive, end-to-end platform to process, analyse, and visualise ST data, all through a user-friendly GUI. VR-Omics is designed to democratise ST data analysis, making it accessible to both bioinformaticians and non-bioinformaticians while generating reproducible results in a timesaving manner compared to traditional coding methods. VR-Omics is platform-agnostic, supporting input data from both sequencing and imaging-based ST technologies, as well as custom ST data matrices [12–14]. VR-Omics primarily functions as a conventional desktop application, with the inclusion of virtual reality (VR) integration as an optional feature (Additional file 1: Video 1). While fully supporting single-slice ST data analysis and visualisation, VR-Omics further facilitates these functions for multi-slice ST data with additional capabilities, including merging or manual alignment of slides and comprehensive 3D visualisation.

Within the framework of ST data processing, following sample preparation, data generation (via sequencing- or imaging-based technologies), and upstream data processing usually done by the vendor, VR-Omics encompasses and executes the downstream analysis steps (Fig. 1a). VR-Omics enables data filtering, cluster analysis, and the identification of spatially variable genes (SVGs), alongside interactive visualisation and the generation of publication-ready outputs such as images, videos, and data files (Additional file 2: Fig. S1).

We demonstrate the utility of VR-Omics through the analysis of both single and multi-slice rare pediatric cardiac rhabdomyomas (cRMs) for which the disease mechanism remains unknown [15, 16]. cRMs are non-cancerous tumours that, while extremely rare in the general population, with a prevalence between 0.0017% and 0.28%, are the most common form of primary pediatric cardiac tumour [17, 18]. Depending on the anatomical presentation of cRMs in cardiac muscle, these tumours can impair normal heart function by causing respiratory distress, arrythmias, ventricular obstructions, and cardiac failure [19, 20]. When their presence leads to severe health complications, treatment options are very limited and include surgical resection [19], which may lead to additional mortality or morbidity complications for the patient [18]. cRMs can be characterized morphologically by the large, cytoplasmic glycogen vacuoles present within cardiomyocytes [21]. To decipher the molecular mechanisms underlying cRM formation, limited transcriptomics studies of 10 marker genes have been performed on these tumours, identifying abnormal regulation of the mTOR signaling pathway associated

with cell proliferation [22]. Abnormal activity of the mTOR pathway has also previously been linked to tumour cells requiring increased anabolic activity to sustain their abnormal growth [23]. Using VR-Omics to analyse multi-slice Visium data generated from these cRMs, we identified transcriptome-wide robust novel transcriptional signatures distributed in discrete niches across the cRM.

Additionally, we showcased the precision of VR-Omics for interactive 3D analysis by performing studying transcriptomic profiles of the mammalian heart by Asp et al. [24], rigorously validating its performance against state-of-the-art ST tools: STitch3D [6], VR-Cardiomics [12], Loupe Browser [25, 26], Xenium Desktop-Explorer [27], MERSCOPE Web-Vizualizer [28], Stereopy [29], SODBView (through its visualiser SOView) [10], and VT3D [7]. The mammalian heart contains spatially restricted genes that display complex spatial expression in the heart sub-compartments [30, 31], for instance the atrial markers *Myl2* and *Myh7* were found to be differentially expressed between the right ventricle and right atrium. To evaluate the 3D multi-slice capability of the current ST algorithms, we performed comparative analysis using a standard workflow designed to cover all the necessary procedures for a typical differentially expressed gene (DEG) analysis. We show that published markers for chamber-specific markers could be faithfully retrieved using the VR-Omics interactive interface compared to command line pipelines.

Finally, we sought expert feedback from ST specialists with experience in analysing 2D and 3D Visium, Xenium, and MERFISH spatial transcriptomics data. This feedback demonstrated that VR-Omics successfully delivers major advantages to users over other benchmark platforms by streamlining the analysis pipeline, presenting an "incredible" visual quality and a "well-designed and user-friendly interface." VR-Omics also accurately captured the same results as other pipelines previously tested by users. "The automated outputs generated by VR-Omics were highly consistent with manual analysis, making it an appealing option for users working with spatial transcriptomics data."

(See figure on next page.)

Fig. 1 Overview of analytical workflows and capabilities of VR-Omics. **a** Schematic representation of the overarching workflow, from the generation of ST data to its inclusion in publications, highlighting the analytical workflows performed within VR-Omics. From left to right, the workflow illustrates sample preparation steps for imaging-based or sequencing-based ST methods. Data typically undergoes initial processing by the vendor before being made accessible to the end-user. The orange section highlights VR-Omics' ability to seamlessly incorporate vendor-processed data, enabling automatic mining through AWs. Processed data can then be visualised and interactively explored in the Visualiser, which provides multiple publication-ready output formats, including images, videos, and files. **b** Schematic overview of data generation through co-planar sectioning and subsequent data processing workflow for multi-slice co-planar ST datasets with VR-Omics. **c** Schematic overview of data generation through 3D workflows from consecutive slide sectioning and subsequent data processing workflow for multi-slice 3D ST datasets with VR-Omics. **d** Gene search functionality of the VR-Omics Visualiser. $\mathbf{d_i}$ Genes can be searched using the search bar. $\mathbf{d_{ii}}$ Example of normalised gene expression visualised in a heatmap-like manner, ranging from low expression (blue) to high expression (red). $\mathbf{d_{iii}}$ Example of normalised binary gene expression, highlighting all locations in green with expression levels exceeding a user-defined threshold. **e** Schematic overview of spatial analysis workflows in VR-Omics for sequencing- and imaging-based technologies producing clustering and SVG results. **f** Interactive visualisation of Xenium breast cancer data [15]. $\mathbf{f_i}$ Visualising of cluster regions of spatial coordinates. $\mathbf{f_{ii}}$ Visualisation of cluster regions on UMAP and t-SNE coordinates. $\mathbf{f_{iii}}$ Automated selection of unique cluster regions through the interactive cluster legend. **g** Schematic of ROI selection using VR-Omics Visualiser. $\mathbf{g_i}$ Schematic representation of selecting locations in 2D or 3D datasets, with up to 4 ROI groups that can be exported. $\mathbf{g_{ii}}$ Visualisation of MERFISH mouse brain data, including selection of individual regions, which can be exported and re-imported into the VR-Omics Visualiser

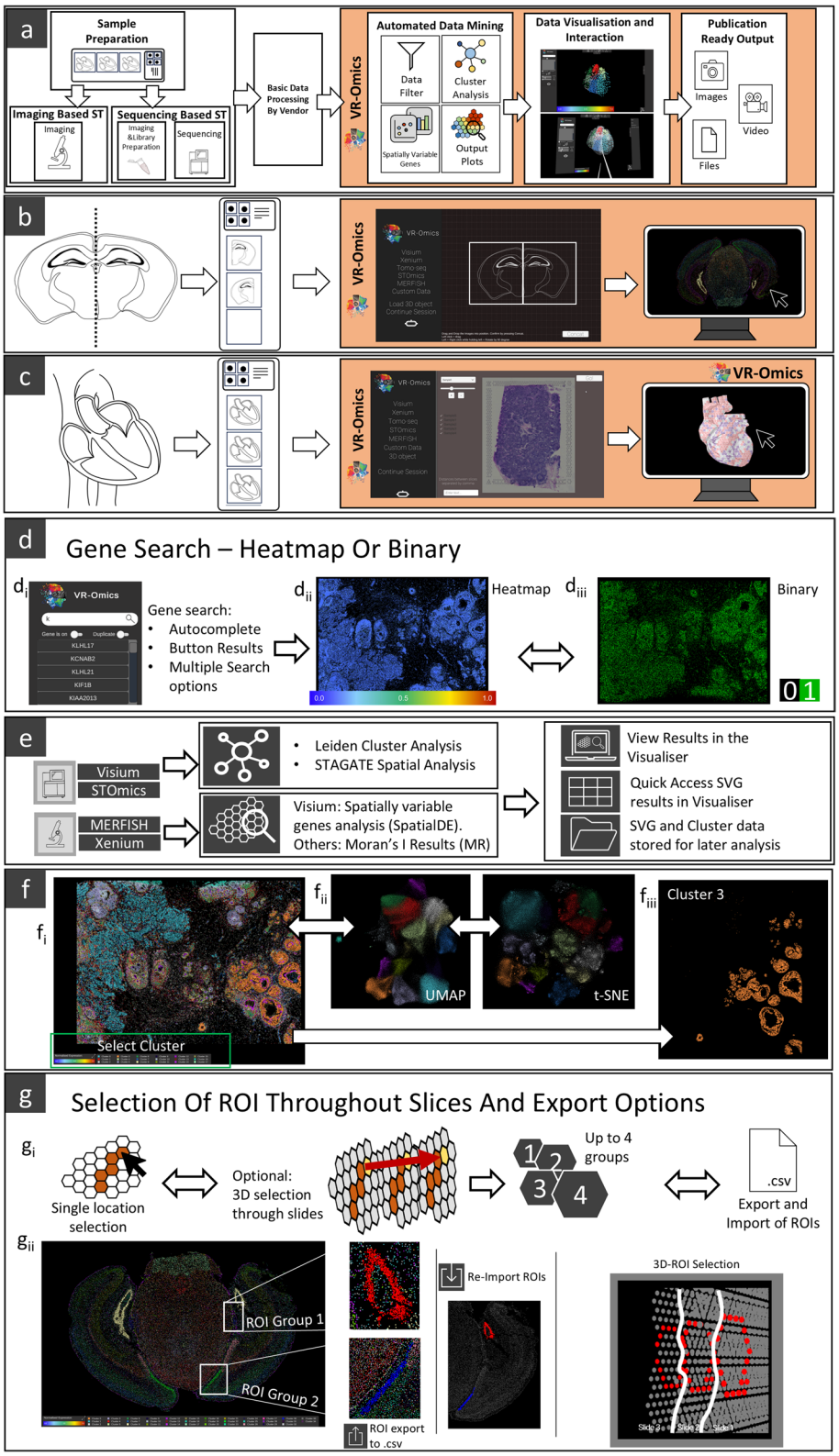

Fig. 1 (See legend on previous page.)

These multifaceted use-cases collectively exemplify the versatility and robustness of VR-Omics as a pivotal tool for effective and novel spatial transcriptomics research.

Results

VR-Omics enables end-to-end ST analyses in 2D and 3D

With VR-Omics, we developed the first automated, interactive tool with a GUI that allows both the concatenation and analysis of multiple co-planar slices, as well as the generation of a harmonised coordinate system of stacked multi-slice tissues in 3D. This integration is achieved through the utilisation of the Unity Gaming Engine [32] combined with Python-based analysis incorporated in VR-Omics as Automated Workflows (AWs) (Additional file 3: Methods).

For the analysis of multiple co-planar slides, we developed a user interface utilizing the Unity Gaming Engine. This interface enables users to visualise and manipulate tissue slides, allowing them to be freely arranged and rotated to approximate the native structure of the tissue (Fig. 1b, Additional file 4: Video 2, 0:36 s). This spatial arrangement is captured in the *world space* of Unity, where the position of the tissue slides relative to each other are meticulously collected. These coordinates are subsequently transferred to a Python-based workflow, which concatenates the data objects according to their spatial alignment. Rotation of the slices is facilitated by applying transformation matrices to the array of data points. Once aligned, the separate data objects are concatenated into a single entity and converted into formats typically compatible with downstream processes (e.g., h5ad, csv). Additionally, the interface provides options for users to customise the filtering and processing parameters necessary for subsequent analysis (Additional file 5: Video 3).

For the analysis of 3D-stacked datasets, we designed a GUI interface that allows users to manually align multiple ST sections of a 3D structure. To achieve this, the Unity-based user interface facilitates the rotation, alignment, and reconstruction of consecutive sections into a cohesive 3D dataset (Fig. 1c) through VR-Omics' Visualiser component. This interface provides tools for precise manipulation, enabling users to set the distances between consecutive slides as well as adjust the rotation of individual slides (Additional file 4: Video 2, 0:15 s). Users can explore 3D datasets dynamically, gaining deeper insights into the spatial organisation and intricate architecture of the tissue, while still generating the static output files (such as those available for 2D datasets) for incorporation into publications or further downstream analysis.

The Visualiser enables comprehensive, interactive exploration of 2D and 3D datasets, allowing users to seamlessly investigate gene expression data. Through a convenient search bar (Fig. 1di), gene expression can be visualised in multiple formats, including a heatmap-like representation (Fig. 1dii) or a binary visualisation (Fig. 1diii). Beyond gene-level visualisations, the platform supports the exploration of spatially relevant data by incorporating purpose-built packages, such as STAGATE [33], for fully automated cluster analysis (Fig. 1e). Additionally, standard clustering algorithm in form of Leiden is included for robust comparative analyses (Fig. 1e).

To further enhance spatial data exploration, we integrated SpatialDE [34], which identifies SVGs. These analyses can be visualised directly within the interface or exported for downstream use. The Visualiser's runtime capabilities extend to dimensional reduction visualisations, such as UMAP and t-SNE. Users can dynamically switch between spatial

visualisation (Fig. 1fi), UMAP (Fig. 1fii), or t-SNE representations, offering flexibility in data interpretation. By interacting with the cluster legend (Fig. 1fi), users can isolate specific clusters for detailed investigation (Fig. 1fiii), with the option to export these subsets as CSV files for further analysis.

An additional feature of the Visualiser is the ability to manually define regions of interest (ROIs) directly within the interactive visualisations. Users can select specific locations (Fig. 1gi) on a single slide, or including for 3D datasets, where the Visualiser can automatically detect and include underlying regions in the ROI selection. This functionality can be toggled on or off, providing tailored control over the analysis. The tool supports the selection of up to four distinct regions simultaneously (Fig. 1gii), which can be exported as CSV files containing gene expression data. These exported ROIs can also be re-imported in future sessions for extended analysis, streamlining workflows and enabling iterative exploration of complex datasets.

These AWs enhanced with the Visualiser's user-friendly interface streamline the analysis of multi-sliced tissue sections by ensuring consistency and robustness throughout the analytical process. By standardizing workflows through containerized pipelines, our software minimises difficulties that could otherwise arise from increased number of analytical steps. This uniform approach ensures reliable and a simplified integration and analysis across slices.

Comparison of VR-Omics to other tools for spatial transcriptomics analysis

To demonstrate the comprehensive capabilities of VR-Omics, we conducted an extensive evaluation on common analysis workflows encompassing data input/export handling, visualisation, and general utility, among a broad spectrum of ST tools outlined in Fig. 2a [6, 7]. We systematically identified the essential steps required for analysing both coplanar multi-sliced tissues and depth-stacked datasets. Our comparison with a diverse array of ST tools revealed that VR-Omics is the only platform capable of executing many of the necessary procedures integral to this analysis (Fig. 2a). However, certain capabilities, such as batch correction, cell segmentation, and spot deconvolution are currently lacking from VR-Omics. These analytical steps cannot be implemented across data generated from all platforms, rendering them a more niche analytical step. However, the number of steps available within the ST analysis pipeline underscores the necessity of a unified platform that consolidates comprehensive data analysis within a single environment, as these tasks often require integrating multiple tools and navigating diverse coding languages such as R and Python (Additional file 6: Questionnaire).

To exhibit VR-Omics' capabilities for analysis and visualisation of ST datasets generated through multiple ST platforms, we performed a high levels cross-platform comparison using a similar biological dataset. Here we analysed and visualised clusters across a mouse brain dataset generated with the Visium, Xenium, STOmics, and MERFISH platforms (Additional file 2: Fig. S2). Despite differences in platform resolution and slight differences in anatomical brain sections displayed, VR-Omics successfully identifies similar spatial patterns and clustering across all four datasets generated with different platforms (Additional file 2: Fig. S3).

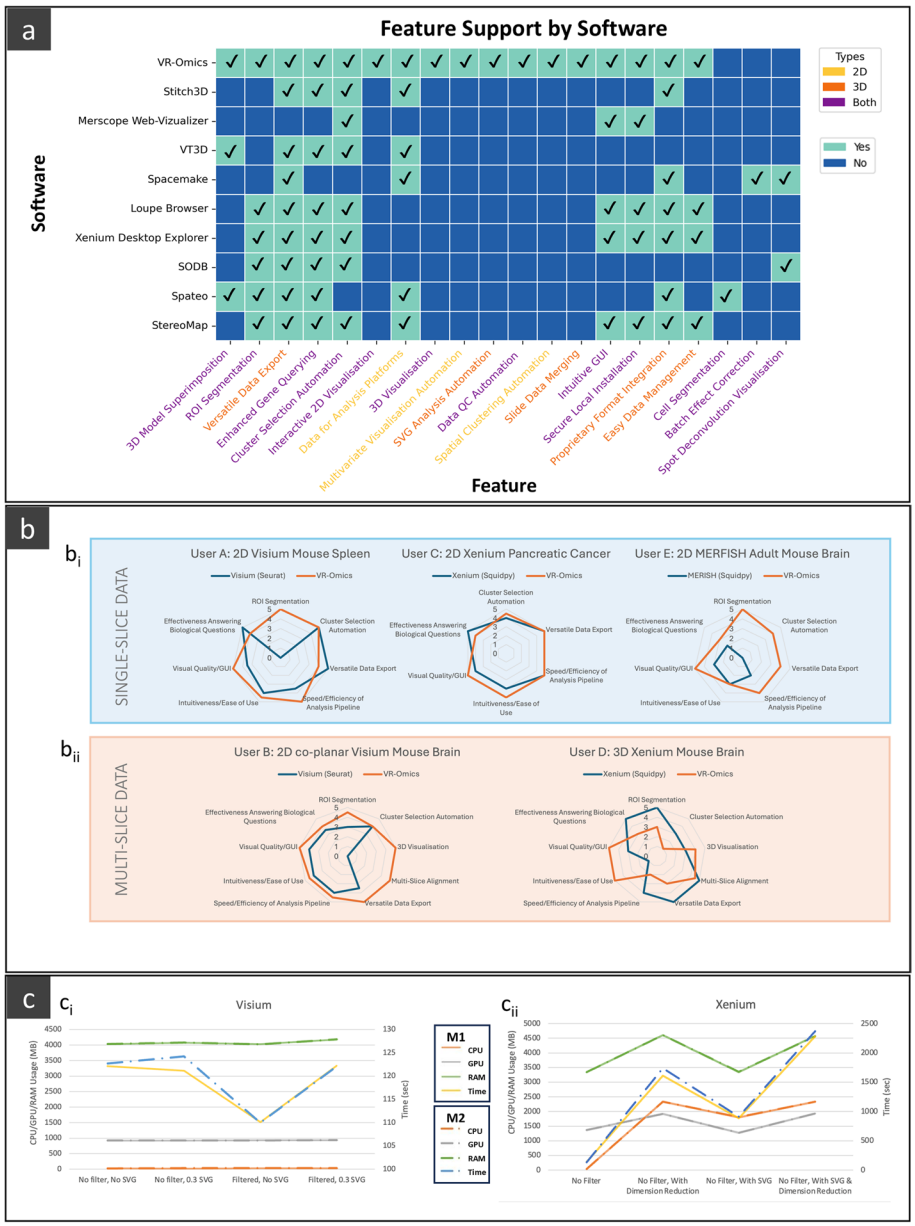

Fig. 2 VR-Omics comparison with existing ST workflows and AWs performance tests **a** Heatmap comparison of analytical features supported by VR-Omics and other available software for ST analysis. Tested software is outlined on the y-axis while analytical features are listed on the x-axis and colored according to their applicability to multi-slice co-planar or 3D stacked datasets. Feature labels are colored on the x-axis according to their availability for solely 2D (yellow) or 3D datasets (orange), or whether this is available for both (purple). The heatmap is then colored according to whether features supported by the specific software are displayed in teal with a tick while unsupported features are displayed in dark blue. **b** Results of the expert user study benchmarking VR-Omics against state-of-the-art workflows. $\mathbf{b_i}$ Results for single-slice users: User A (Visium single slide, mouse spleen) VR-Omics compared to Seurat, R analysis workflow, User C (Xenium single slide, pancreatic cancer) VR-Omics compared to Python package Squidpy, and User E (MERFISH single slide, adult mouse brain) VR-Omics compared to Python package Squidpy. $\mathbf{b_{ii}}$ Results for multi-slice users: User B (Visium co-planar slides, mouse brain) comparing VR-Omics and R analysis workflow in Seurat and User D (Xenium 3D mouse brain) comparing VR-Omics and Python package Squidpy. **c** Performance test results of AWs, showing time, memory, and RAM usage across different workflow settings for two replicates. $\mathbf{c_i}$ Performance results for Visium: (1) no filter, no SVG; (2) no filter, with SVG; (3) filter, no SVG; and (4) filter, with SVG. $\mathbf{c_{ii}}$ Performance results for Xenium: (1) no filter; (2) no filter, with dimensionality reduction; (3) no filter, with SVG; and (4) no filter, with both SVG and dimensionality reduction

VR-Omics expert feedback

Five independent experts familiar with different ST platforms but first-time VR-Omics users participated in a systematic assessment of how VR-Omics performed compared to non-automated approaches for data analysis. Two experts analysed Visium data (single slide and concatenated co-planar datasets respectively), two experts analysed Xenium data (single slide and 3D datasets respectively), and one expert analysed MERFISH data (single slide) (Fig. 2b).

All experts commented on the ease of using VR-Omics compared to their default platforms, highlighting the streamlined analysis pipeline, which required no coding background to navigate, as a key advantageous feature (Additional file 6: Questionnaire). One expert remarked "Loading the input and starting the analysis were very straightforward thanks to the streamlined pipeline" while another said, "The software is user-friendly and well-suited for users with limited bioinformatics experience, providing a straightforward way to gain a preliminary overview of the data."

VR-Omics consistently scored a rating of 5/5 from all experts for its "Visual Quality/GUI" while its "Intuitiveness/Ease of Use" was rated higher than or equal to the benchmark platforms by all users (Fig. 2b). VR-Omics' "Speed/Efficiency of Analysis Pipeline" and "Cluster Selection Automation" were rated as equivalent or better than benchmark platforms by four out of five experts.

One expert analysing multi-slice data rated VR-Omics "3D visualisation" and "Multi-Slice Alignment" 5/5 remarked "I like the way the software visualises the concatenated slices. Very impressive." They also commented that these features were not available in SpatialBenchVisium [35] which "showed limited support for slice concatenation" (Additional file 6: Questionnaire). A second expert analysing 3D data "loved the interaction" possible, rating VR-Omics' "3D Visualisation" higher than Xenium and scoring VR-Omics "Multi-Slice Alignment" 4.5 compared to Xenium's 5.

Three out of five experts rated the benchmark platform higher for "Effectiveness Answering Biological Questions" identifying a lack of annotation "doesn't identify specific cell types and markers," and limited customisation of analysis output as the main features requiring improvement (Fig. 2b, Additional file 6: Questionnaire). "Without annotation, interpretation remains challenging beyond visualising the spatial expression patterns of genes of interest." While the software is excellent for getting started, further in-depth or manual analyses are necessary to address specific biological questions.

Experts reported that they were able to retrieve similar results using the VR-Omics pipeline "The outputs were nearly identical, largely due to the use of the same Squidpy analysis framework." This was as expected for Xenium users given that Squidpy was used as the backends of VR-Omics' AW. "Since the same analysis framework is employed, the automated outputs generated by VR-Omics were highly consistent with manual analysis, making it an appealing option for users working with spatial transcriptomics data." SpatialBenchVisium [35] users remarked that they observed "similar genes among the top SVGs" and "clear clusters corresponding to expected main regions/structures that are expected in spleen during malaria infection."

VR-Omics performance tests

We further benchmarked VR-Omics AWs performance against ST platforms Visium and Xenium (Fig. 2c, Additional file 7: Table S1). These tests assessed processing time, memory usage, and RAM consumption, with results based on two replicate measurements.

For Visium datasets, processing times ranged from ~110 s for standard processing (without filtering, SVG, or dimensional reduction) to ~125 s when performing SVG analysis (Fig. 2ci, Additional file 7: Table S1). This measurement used a dataset containing ~5000 locations, which represents the maximum size of a standard Visium experiment, constrained by the 5000 barcoded spots available on the platform.

For Xenium datasets, processing times for standard analysis were 135 s for a dataset containing 167,782 locations. As expected, more complex analyses, including SVG, required around 15 min, while the full analysis—incorporating filtering, SVG, and dimensional reduction—took approximately 39 min (Fig. 2cii, Additional file 7: Table S1).

For MERFISH datasets, VR-Omics AW measurements aligned closely with those from Xenium AW due to the use of the same core analysis packages, primarily Squidpy, and consistent methods for dimensional reduction and SVG detection (Moran's *I*). Processing times ranged from ~84 s for standard analysis to just under 10 min for full analysis, including clustering, SVG identification, and dimensional reduction, for a dataset containing approx. 78,000 spatial locations (Additional file 7: Table S1).

Furthermore, except for Xenium datasets which required ~39 min to run a full processing pipeline, generally there is a small difference between running pipeline purely for visualisation or running a pipeline selecting all analysis options, including SVG identification and clustering. This was further emphasised by responses in the expert feedback, which stated that when analysing Xenium data "The entire analysis was completed in under 30 min, including clustering, visualisation of top genes defined by Moran's I score, neighborhood enrichment, and co-occurrence scoring."

We also note that changes in clustering resolution does not greatly affect processing time or memory requirements. The largest requirements were for a Xenium dataset requiring just under 40 min processing time with 167,782 locations. Additionally, we tested multi-slice visualisation capabilities for Visium up to 2048 slides which included 5,533,696 locations (Additional file 8: Table S2). Even at this large experimental size, visualisation was possible after a significant lag and rendered data interaction difficult, indicating the significant upper limits of VR-Omics current capabilities to handle large datasets (Additional file 8: Table S2). Conversely, only ~0.58 s were required to visualise a single Visium datasets filtered to 2702 locations (Additional file 8: Table S2).

Benchmarking VR-Omics 3D reconstruction workflow

To illustrate the capabilities of VR-Omics in comparison against multi-slice ST tools, we designed and performed a standardised workflow to analyse a 3D multi-sliced dataset derived from the developing human heart at 6 days post coitum (dpc) by Asp et al. [24] (Fig. 3a, Additional file 9: Table S3). The workflow included: (1) inputting ST data; (2) clustering spots/locations; (3) assembling slices into a 3D structure; (4) manually selecting two ROIs; and (5) identifying the top DEGs between these ROIs (Fig. 3a). This

approach is critical for unraveling spatial gene expression patterns and comprehending the architectural complexities of tissues, where preserving the native 3D context is crucial for understanding the developmental intricacies that shape complex organ structures such as the heart. To standardize the comparison, we employed the same bioinformatics methods for identification of DEGs for all tools compared.

We conducted this workflow comparing VR-Omics against several other tools: STitch3D [6], VR-Cardiomics [12], Loupe Browser [25, 26], Xenium Desktop-Explorer [27], MERSCOPE Web-Vizualizer [28], Stereopy [29], SODBView (through its visualiser SOView) [10], and VT3D [7] (Fig. 3b, Additional file 9: Table S3, Additional file 3: Methods). Each tool was evaluated based on its ability to complete each workflow step, with scores assigned for full (score = 1), partial (score = 0.5), or unsuccessful (score = 0) execution. Here partial execution refers to relying on additional custom code, executed outside of the tool, required to execute this step.

Firstly, the comparative analysis underscored that most tools are tailored primarily for 2D data, with limited capabilities for integrating 2D slices into a coherent 3D structure. Therefore, Loupe Browser, Xenium Desktop-Explorer, MERSCOPE Web-Vizualizer, Stereopy, and SODBView were excluded from further comparison (Additional file 2: Fig. S3a). VR-Omics successfully completed all five steps (Fig. 3bi); however, VT3D (Fig. 3bii), VR-Cardiomics (Fig. 3biii), and Stitch3D (Fig. 3biv) could not proceed beyond completing task three (assemble slices). Secondly, while VT3D and STitch3D support the assembly of 2D slices into 3D (Fig. 3bii and b_{iv}), they lack functionality for native 3D ROI selection, limiting the ability to isolate and investigate spatially restricted cell populations across the 3D stack. ROI selection in 3D (step 4) is fully supported by VR-Omics (Fig. 3bi). Thirdly, our previous tool, VR-Cardiomics, facilitates steps 3 to 5 of the workflow but is constrained by its inability to perform steps 1 and 2, to process novel input data and perform clustering, highlighting VR-Omics' unique flexibility and comprehensive support for 3D ST data analysis [12] (Fig. 3bi and b_{iii}). Notably, only VR-Omics

(See figure on next page.)

Fig. 3 Cross-platform comparison of the workflow for 3D reconstruction of the developing human heart dataset. **a** Schematic of the steps involved in the workflow to identify DEGs between different regions of interest (ROIs) of a 3D dataset. This workflow compares gene expression between the right atrium and right ventricle. **b** Overview of the results from each software's workflow to reconstruct the 3D dataset of the developing heart, delineate the right ventricle and right atrium, and find DEGs between them. Includes a visualisation of the ROIs selected as the right ventricle (red) and right atrium (blue). On the right under scoring a spider plot displays a score out of five for how many of the workflow steps the software can complete. Both software available with a GUI and software requiring coding skills are tested. **b_i** Results from VR-Omics completing the 3D reconstruction workflow aiming at generating a list of DEGs between right ventricle and right atrium. On the left the final visualisation of the right atrium (blue) and ventricle (red) are displayed within the VR-Omics GUI and the spider plot on the right displays VR-Omics ability to complete all 5 steps of the workflow. **b_{ii}** Results from VT3D executing the workflow. On the left the final visualisation of the right atrium and ventricle is displayed in a plot generated with VT3D and the spider plot on the right displays scoring 4.0 out of 5.0, requiring additional coding for 2 out of the 5 tasks. **b_{iii}** Results from VR-Cardiomics executing the workflow using a mouse heart, with the chambers displayed on the left and the spider plot on the right displaying the 3.5 steps that can be completed within VR-Cardiomics, requiring additional coding for incorporating input data. **b_{iv}** Example results from Stich3D executing the workflow with chambers displayed and colored on the left and the spider plot on the right. Selection of specific ROIs to highlight the right atrium in black and right ventricle in red performed in R outside of the STich3D framework. **c** Time required for VR-Omics to visualise exponential numbers of multi-slide Visium datasets. This demonstrates VR-Omics capabilities to effectively visualise even large datasets

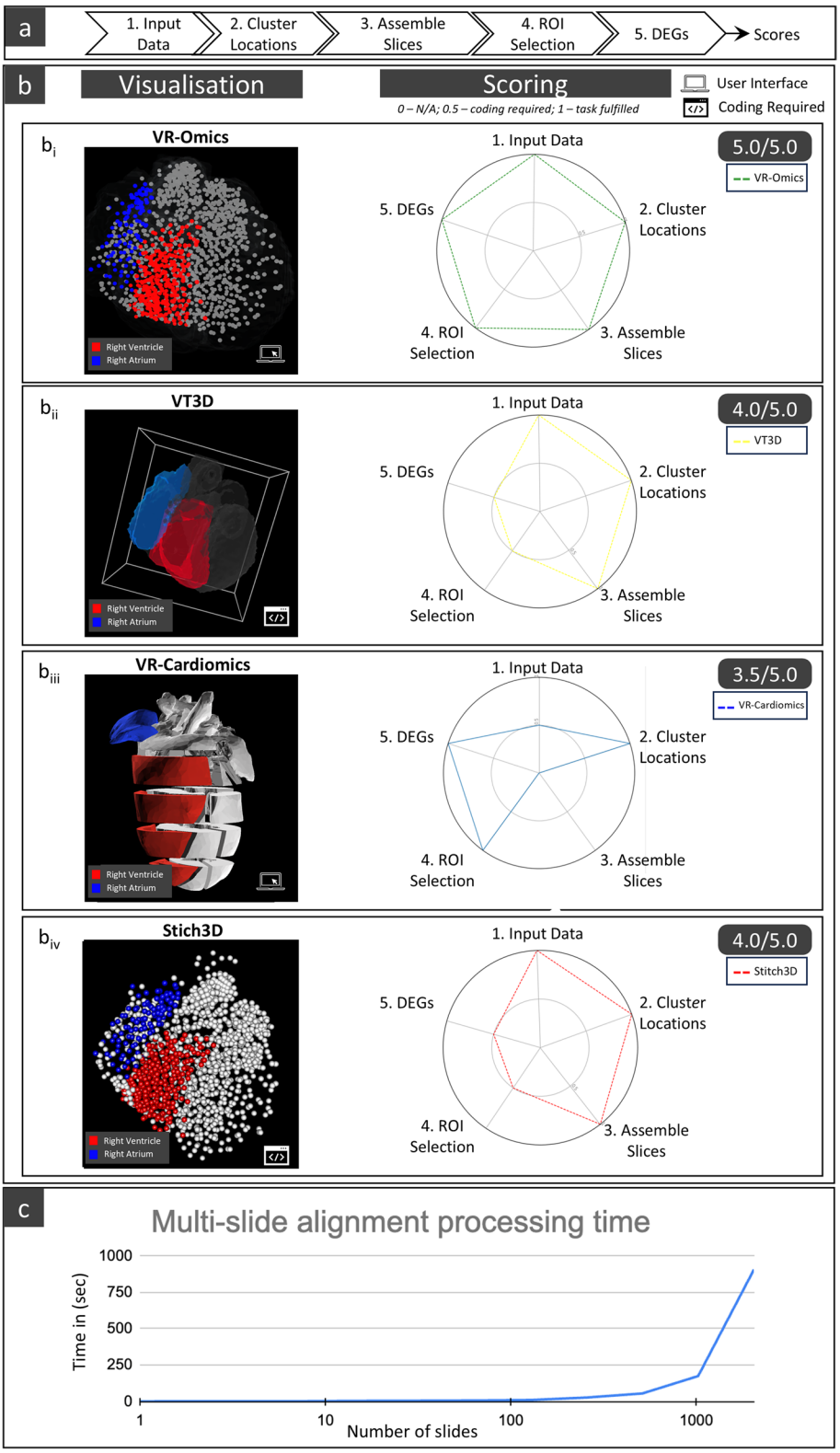

Fig. 3 (See legend on previous page.)

achieved a perfect score across all five steps, showcasing its unparalleled capacity for conducting comprehensive 3D spatial analyses and DEG identification (Fig. 3bi, Additional file 2: Fig. S3b, Additional files 10–11: Tables S3 and S4). To showcase the ease of selecting 3D anatomical regions in VR-Omics, we repeated the analysis conducted by Mohenska et al. [30] which identified DEGs (including *Myl2* and *Myh7*) between the right ventricle and right atrium in the adult mouse hearts. We employed two independent datasets from the developing human heart by Asp et al. [24] and the adult human heart by Litviňuková et al. [31], and performed a similar right ventricle vs. right atrium analysis, using VR-Omics alongside similar spatial transcriptomics tools (Stitch3D, VT3D, VR-Cardiomics). By enabling 3D ROI selection, VR-Omics could generate the DEGs between right ventricle vs. right atrium, which included markers genes such as *Myl2* and *Myh7* (Additional file 2: Fig. S3, Additional files 10–11: Tables S3 and S4). This consistency with the DEGs revealed by Mohenska et al. [30] demonstrated that VR-Omics correctly selected the 3D regions of interest, a feature not available in other ST tools at the time of this study (Fig. 3).

Understanding molecular signatures of pediatric cardiac rhabdomyomas using VR-Omics

To further illustrate VR-Omics' unique end-to-end capabilities in the analysis of multi-slice datasets, we tested it on a multi-slice co-planar dataset to interrogate a disease mechanism that has not previously been transcriptomically investigated. To elucidate the molecular and cellular perturbations leading to these abnormal cell populations and to explore tumour heterogeneity in a spatial context, we profiled multiple cRMs with 10X Genomics Visium platforms and VR-Omics.

A total of four cRMs were obtained from three separate patients. The first sections were obtained from patient MCHTB302 diagnosed with Birt-Hogg-Dubé syndrome (BHDS) who had two cRMs, one in the left ventricular cavity and a second in the apex of the heart (Fig. 4ai). This patient was known to be heterozygous for a mutation in *FLCN*, previously linked to BHDS, that causes a ~ 30% reduction in the production of FLCN

(See figure on next page.)

Fig. 4 Analysis of multi-slice co-planar cRM datasets within the VR-Omics framework. **a_i** Schematic representing location of cRM from patient MCHTB302 used for data generation with the Visium platform. **a_{ii}** Electrocardiogram displaying location of cRM in left ventricular cavity. **a_{iii}** Schematic representing approximate locations of sections taken for data generation using the 10X Genomics Visium platform. **a_{iv}** Immunostaining of normal myocardium on edge of tumour, highlighted in red box, and tumour cells towards center. Ki67 indicates proliferation within the tumour (orange); nuclei staining (Hoechst, blue); cardiac troponin T (cTNT, green). **b_i** Example of concatenation interface available within VR-Omics for multi-slice Visium datasets. **b_{ii}** Example of filtering parameters available with VR-Omics user interface. **b_{iii}** Example of VR-Omics menu within the Visualiser for exploration of gene expression across multi-slice dataset. MCHTB302 cRM data is visualised with expression of *ATP5IF1* displayed. **c_i** Reconstruction and concatenation within VR-Omics of 3 co-planar, H&E stained slices separated onto different Visium capture areas due to size of the tissue. **c_{ii}** Example of STAGATE clusters visualised across the reconstructed multi-slice MCHTB302 co-planar dataset within VR-Omics. **c_{iii}** GO analysis results of multi-slice co-planar dataset using the STAGATE cluster markers as inputs for Metascape. Oxidative phosphorylation and aerobic respiration signatures are highlighted in a red box for clusters 0 and 4 located at the center of the tumour. **d_i** Reconstruction and concatenation within VR-Omics of 2 co-planar, H&E stained slices MCHTB362 atrial cRM data separated onto different Visium capture areas due to size of the tissue. **d_{ii}** Example of STAGATE clusters visualised across the reconstructed co-planar dataset within VR-Omics. **d_{iii}** GO analysis results of multi-slice, co-planar dataset using the STAGATE cluster markers as inputs for Metascape. Oxidative phosphorylation and cellular respiration signatures are highlighted in a red box for clusters 2, 3, and 6 located at the center of the tumour

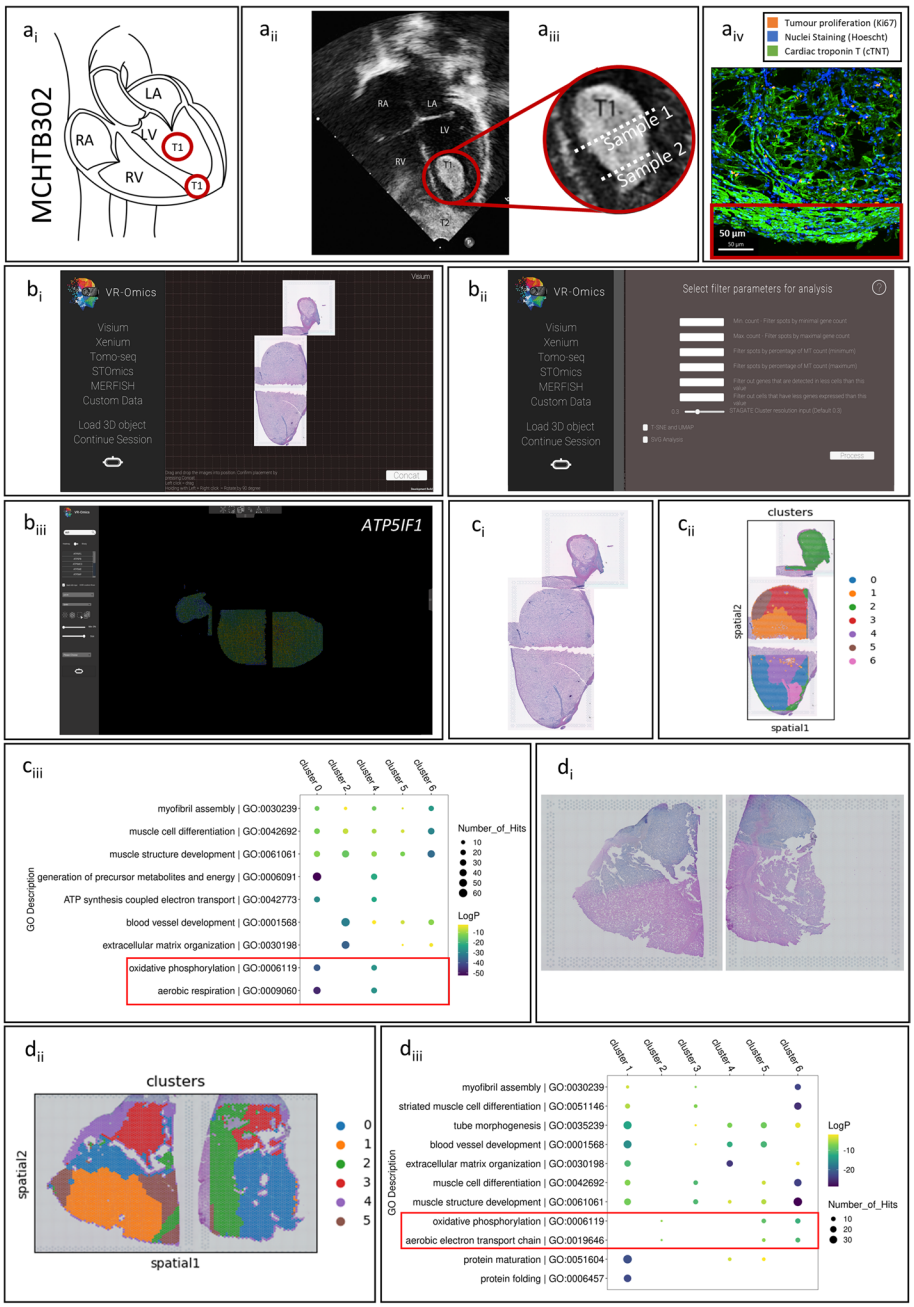

Fig. 4 (See legend on previous page.)

compared to wild type due to proteasomal degradation [16, 36]. This gene may be key in understanding underlying mechanisms of tumour formation or maintenance, as FLCN has also been shown to form a complex with FN1P1 and/or FN1P2 as well as AMPK, which plays a key role in regulating cell metabolism through the AMPCK-mTOR pathway [37–39]. For this study, two sections were taken from the cRM located in the left ventricular cavity (Fig. 4aii–iii). Initial immunofluorescence staining performed on this tumour indicated evidence of proliferating cardiomyocytes through colocalized staining of cTNT and Ki-67 (Fig. 4aiv) [40]. This proliferation was specific to the center of the

tumour and associated with vacuolised cardiomyocytes while the expression of Ki-67 was absent from the surrounding, normal myocardium around the edge of the tumour (Fig. 4aiv). Therefore, we sought to identify transcriptional differences that may assist in the proliferation or maintenance of the abnormal cardiomyocytes located at the center of the tumour.

Due to the size limitations of the Visium capture area, the section originating from the center of the tumour was then divided across 3 Visium slides (Fig. 4bi). The 3 slides were easily and quickly recombined using VR-Omics' unique, interactive multi-slice concatenation to generate a single data object from the multi-slice, co-planar dataset that more faithfully recapitulated the biological sample (Fig. 4bi, Additional file 4: Video 2, 0:36 s). Once loaded and concatenated, data cleaning can now be performed across the joint multi-slice dataset using a variety of parameters, and analytical steps such as SVG identification and inclusion of t-SNE and UMAP plots chosen within the VR-Omics framework (Fig. 4bii). Once processed and analysed, the dataset can be uploaded into the VR-Omics Visualiser for the user to interact with and mine for biological information (Fig. 4biii).

To better understand the nature of these cRMs, we sought to identify distinct transcriptional signatures within the cell populations of the cRM that would align or provide further information to the matched histological image (Fig. 4ci). Using the STAGATE algorithm for clustering (within VR-Omics' AW) (Fig. 4cii) and Scanpy for marker identification, we identified cell populations (clusters 0 and 4) in this dataset that displayed a switch in cellular metabolism to increased aerobic respiration and oxidative phosphorylation when all the markers from these clusters (e.g., *ACO2*, *ATP5F1A*, *ATP5F1B*, *ATP5ME*, *COX4I1*) were used as an input for a gene ontology enrichment analysis with Metascape (Fig. 4ciii, Additional file 2: Fig. S4). Overall, the lower of expression of these markers in clusters 2, 3, and 5 of the tumour compared to other clusters indicates their specificity to the abnormal cardiomyocytes rather than to the primarily fibrotic capsule (Additional file 2: Fig. S4). This is also in line with the restricted expression of Ki67 to the abnormal cardiomyocytes in the center of the tumour (Fig. 4aiv). These populations may generate additional ATP through upregulation of genes such as *ATP5IFI*, paralleling aspects of the Warburg effect which sustains abnormal cell proliferation in cancerous tumours [41] (Additional file 2: Fig. S4 g). These findings are in line with metabolic changes observed in murine models with mutated or knocked out *FLCN*, similar to the patient's genotype leading to a lower expression of *FLCN*, that are proposed to be due to the dysregulation of the AMPK-mTOR pathway [42, 43]. Furthermore, we can see relatively low levels of *FLCN* expression across these tumour sections (Additional file 2: Fig. S5a). *FLCN* is implicated in other cardiac diseases such as cardiac hypertrophy and therefore may be one of many dysregulated genes giving rise to cRMs [43]. Other evidence suggests *FLCN* plays a role in cardiac homeostasis and this lack of cellular energy level regulation may be driving the abnormal proliferation of cardiomyocytes within the cRMs [43].

We undertook multiple avenues of orthogonal validation for these transcriptomic signatures. First, comparable signatures of upregulation of oxidative phosphorylation and aerobic respiration were found in a single slide dataset also taken from patient MCHTB302 (Additional file 2: Fig. S6 and Additional file 11: Results), demonstrating the

consistent presence of this signature throughout the tumour. Secondly, using the same VR-Omics pipeline we identified the same signatures for upregulation of aerobic respiration and oxidative phosphorylation during the individual analysis of sections comprising the multi-slice analysis (Additional file 2: Fig. S7). Therefore, we demonstrate that VR-Omics provides a unique capacity for analysing co-planar datasets to explore novel biological mechanisms in rare tissue sections. Thirdly, similar signatures were also observed when performing a comparable multi-slice analysis using BayesSpace workflow (Additional file 2: Fig. S8a).

We were fortunate to have access to additional multi-slice samples from a second patient to investigate the presence of the transcriptional signature across cRMs with distinct etiologies. We expanded our analysis to samples from patient MCTHB362 who presented with two cRMs, in the left atrium and atrial valve (Fig. 4d, Additional file 2: Fig. S8b_i), and whose father was a known carrier of TSC. Like the cRMs resected from patient MCHTB302, tissue from both cRMs had to be sectioned to accommodate Visium size restrictions and were later virtually reconstructed within VR-Omics; additionally, a small single slice of the cRM was included for analysis (Fig. 4ci and d_i, Additional file 2: Fig. S8b_i–c_i). This allowed direct comparison of multi-slice, co-planar datasets between patients to determine if similar signatures were present. In this instance, we noticed that the cRMs originating in the atria had a slightly different transcriptional profile than previous ventricular samples (Fig. 4ci and d_i). This is also evidenced in the difference in *FLCN* expression across the tumour samples taken from this same patient compared to those from MCHTB302 and MCHTB361 (Additional file 2: Fig. S5). However, upregulation of aerobic metabolism in certain clusters remained constant across this additional multi-slice dataset taken from MCHTB362, demonstrating a consistent association with the tumour phenotype across all patients (Fig. 4dii–d_{iii}, Additional file 2: Fig. S8, and Additional file 11: Results). Processing and visualisation of multi-slice samples through VR-Omics facilitated the discovery of similar cell populations and molecular signatures in MCTHB302 and MCHTB362 that suggest they are characteristic of cRMs (Fig. 4 and Additional file 2: Fig. S8). These findings across patients were further orthogonally validated outside of the VR-Omics framework using a BayesSpace multi-slice analysis workflow (Fig. 5, Additional file 3: Methods, and Additional file 11: Results). These findings suggest that upregulated aerobic respiration is a characteristic transcriptional signature of cRMs (Fig. 4, Additional file 2: Figs. S8–S9).

A final validation step included repeating the same analysis performed on multi-slice samples on separate individual sections for samples taken from both MCHTB302 and MCHTB362. The clustering performed across multi-slice samples reveals additional transcriptional heterogeneity that was not identified when the same analysis was run on individual sections separately (Fig. 4, Additional file 2: Figs. S7, S10, and S11). Of note, when previously concatenated sections from MCHTB362 were analysed separately, a cluster belonging to a seemingly fibrotic capsule along the perimeter of the tumour visible in the joint analysis in Fig. 4dii and Supplementary Fig. 8c could not be identified when the same samples were analysed as individual sections (Additional file 2: Figs. S10 and S11). The joint signature of upregulation of aerobic respiration and oxidative phosphorylation was also only visible in one of the sections, displaying how the

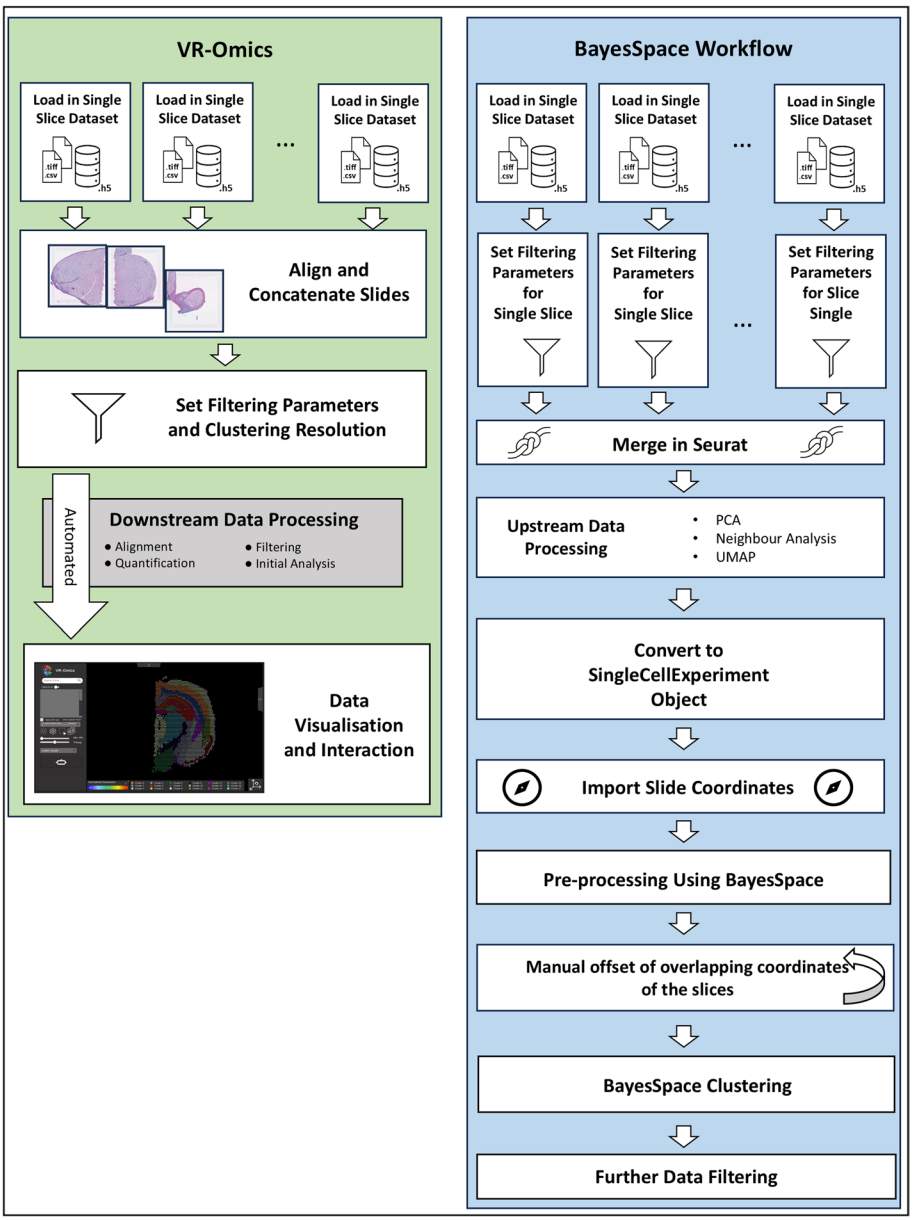

Fig. 5 Schematic outlining different steps in the analytical workflow for processing multi-slice Visium slices in VR-Omics (green) compared to a manual workflow using BayesSpace (blue). Within VR-Omics, boxes outlined in gray indicate steps undertaken by the AW, therefore not requiring user interaction

multi-slice analysis uncovers additional transcriptional heterogeneity (Additional file 2: Figs. S10–S11).

Here we undertook multiple avenues for validation, through the identification of signatures in intra- and interpatient samples along with validating signals present outside of a multi-slice analysis framework. The ability to generate a single data object across multiple planar Visium sections allowed for a better understanding of the distribution of cell populations across the tumour, which would have otherwise been lost due to artificial tissue separation across capture areas (Fig. 4ci and di_i). VR-Omics' GUI makes this process easy and intuitive by simplifying data joining to a simple "drag and drop"

alignment exercise of Visium slices within the VR-Omics' GUI, eliminating the need for computational steps to generate a single data object (Fig. 4bi and Additional file 1: Video 1). A VR-Omics user commented that their Visium data (co-planar slices) were "beautifully aligned" and that "I like the way the software visualises the concatenated slices. Very impressive." emphasising VR-Omics effectiveness in accomplishing this task (Additional file 6: Questionnaire 1). Furthermore, we demonstrate the ease of using an automated multi-slice workflow in VR-Omics providing an interactive data visualiser rather than using a comparable multi-slice workflow in BayesSpace (Fig. 5). VR-Omics minimises the number of steps undertaken by the user for concatenation of multi-slice data and automates many of the pre-processing steps compared to workflows like BayesSpace (Fig. 5), reducing the overall time needed for analysis while, as demonstrated above, generating comparable biological results. Furthermore, VR-Omics circumvents the need for the user to navigate multiple complex analysis packages and overcomes data format compatibility issues by providing an end-to-end comprehensive pipeline for analysis (Fig. 5).

Discussion

The number of experiments generating ST data, as well as the number of locations per dataset, is growing rapidly [44], simultaneously presenting great opportunities for spatial biology investigation and data science challenges. To address the lack of technologies capable of handling multi-slice data, VR-Omics was designed from the ground up to manage multi-slice ST data (both co-planar and 3D stacked) through an intuitive, customizable graphical interface that requires minimal computational skills (Additional file 2: Fig. S1, Additional file 4: Video 2). VR-Omics is designed as a locally installed application, focusing on accessibility especially for users without programming knowledge rather than relying on high-performance computing resources, which can be less accessible. Consequently, features like cell segmentation and spot deconvolution, which often demand significant computational resources, are not supported. However, when compared to multiple tools and pipelines (Stitch3D, Merscope Web-Vizualizer, VT3D, Spacemake, Loupe Browser, Xenium Desktop-Explorer, SODB, Spateo, and StereoMap) for ST data analysis, VR-Omics demonstrates its unique capability in performing comprehensive and advanced end-to-end data analysis for multi-slice ST datasets. Benchmarking VR-Omics against most common ST data analysis and visualisation tools using the 3D developing human heart dataset reveals that only VR-Omics fulfills all the necessary criteria for end-to-end analysis and visualisation typically of interest to biologists in a 3D stacked dataset.

Expert feedback identified the GUI, ease-of-use for users without a coding or computational background, and the visualisation and concatenation feature as major advantages of VR-Omics over existing analysis pipelines. We hope that increased utilisation of VR-Omics will lower the steep barriers of entry, making this platform accessible to people who lack computational experience, democratising the analysis of spatial transcriptomics data. Key areas identified by respondents for future improvements were the lack of customisation within the data/plot exports and the need for further annotation, e.g., no cell type deconvolution available. Several enhancements are already in development and will be released as updates later this year, including automated 3D cluster selection,

more detailed location-specific information (e.g., *p* value display), and the integration of advanced third-party packages for spatial clustering and SVG analysis. In addition, we have improved the GUI and documentation to address features that users struggled to locate during the consultation. With the emphasis on processing of multi-slice 2D and 3D datasets, we tested VR-Omics capabilities to process and visualise datasets generated from different ST platforms. These measurements were conducted without parallelisation, with processes running in the background to enable continued user activity during analysis. While these results demonstrate VR-Omics' ability to efficiently process large datasets, further improvements in processing time can be achieved by executing multiple workflow instances in parallel. This parallelisation approach would be especially beneficial for handling the simultaneous processing of multiple samples, thus enhancing throughput in large-scale studies.

The space of ST data analysis urgently requires applications developed for 3D datasets to align, visualise, and process multi-sliced data. At the time of writing, to our knowledge, only STich3D [6], VT3D [7], and OpenST [45] and our previous work VR-Cardiomics [12] support 3D data visualisation and analyses besides VR-Omics. However, these applications focus on delivering specific aspects of the analytical pipeline and therefore lack critical features to enable end-to-end analysis for users with a range of computational expertise. For example, VR-Cardiomics lacks the ability to analyse users' novel data, rather it focuses on the visualisation of a singular pre-processed dataset, thus preventing its inclusion in future studies. OpenST focuses on providing a platform and framework for data generation, while providing limited 3D data analysis functionality [45]. Thus, we have developed VR-Omics to bridge this gap, allowing users to analyse and interact with their own 3D data in an intuitive manner.

Our comparative analysis between VR-Omics and other proprietary and open-source tools for ST multi-slice analysis (Fig. 2a) reflects a wide range of support for various ST platforms and the advanced analytical tasks required by researchers. Despite the inclusion of tools specialised for enhancing spatial analysis in three dimensions, such as Stitch3D and VT3D, which primarily focus on visualisation and data mining (i.e., analysis of ST data using an array of bioinformatic methods implemented in VR-Omics), only VR-Omics was able to complete all five essential steps for a comprehensive analysis (Fig. 3, Additional file 12: Table S5). This evaluation confirmed VR-Omics' unique ability to support a complete analytical workflow, significantly outperforming existing methodologies in efficiency and thoroughness of data analysis. VR-Omics' singular success in completing all steps of the biological case study, particularly in identifying DEGs that characterise unique transcriptional signatures of two cardiac regions, further highlights its unparalleled capability to provide a robust and comprehensive framework for analysing complex spatial transcriptomics data.

Through the analysis of rare cRM samples, we demonstrate that VR-Omics overcomes two major challenges in multi-slice co-planar ST data: (1) biologically adjacent samples being separated for processing which need to be merged for analysis and (2) inter-sample comparisons. VR-Omics' capability to analyse multi-slice datasets and easily perform inter-sample comparisons permitted the elucidation of key molecular mechanisms contributing to the growth of rare cRM tumours. The workflow available within the VR-Omics framework identified shared signatures of increased aerobic respiration

across patients within abnormal cardiomyocytes faster than comparable workflows implemented across multiple disaggregated packages. This indication of potential dysregulation of the AMPK-mTOR pathway is known to have an effect on mitochondrial metabolism and has been demonstrated in murine models with mutations in *FLCN*, which is homologous to the same gene known to be mutated in patient MCHTB302 [43]. Without platforms for the generation of ST data and tools for its effective analysis through framework tools such as VR-Omics, rare clinical samples preserved in FFPE such as these cRMs (prevalence 0.0017%–0.28%) would remain largely inaccessible. The need for specialized bioinformatics tools and computational skills makes analysis of these rare samples and others like them challenging and inaccessible to many researchers. VR-Omics overcomes these barriers by empowering biologists and facilitating analysis for bioinformaticians.

Conclusion

Multi-slice ST data analysis is quickly evolving and the need for tools to support this is growing [46], and VR-Omics rapidly evolves to address development and improvement cycles. VR-Omics natively supports multi-slice ST data from Visium, Xenium, Stereo-Seq, and MERFISH, Nanostring (CosMX) and visualisation capabilities for Slide-Seq V2. VR-Omics modularity facilitates the future incorporation of new platforms such as VisiumHD. By addressing existing computational limitations in current multi-slice ST tools, VR-Omics offers unique advantages as demonstrated in this study using both stacked 3D and co-planar 2D multi-slice datasets. In this study, we leverage VR-Omics to dissect the mechanisms underlying the growth of pediatric cRMs. Our discovery unlocks potential insights into the regeneration of cardiac muscle for therapeutic purposes as the tumours develop within striated muscle and cause abnormal levels of proliferation after birth. VR-Omics stands out from other tools with unique software architecture, an immersive environment, cross-platform compatibility, and a fully AW, all aiming at simplifying and democratising ST analyses in the spatial biology community.

Methods

VR-Omics architecture

To deliver a seamless user experience, VR-Omics was conceived as a sophisticated end-to-end analysis tool, integrating two primary components via a user-friendly interface (Fig. 1a). The first component, the purpose-built AW, focuses on the processing and mining of raw ST data (Fig. 1a). The second component, the Visualiser, utilizes the processed data to facilitate advanced data visualisation, equipped with multiple features for enhanced data interaction and exploration through a fully interactive interface, designed with intuitive data mining processes in mind (Fig. 1a).

VR-Omics was developed utilising the Unity Game Engine by Unity Technologies, starting with Unity version 2019.4.26f1 [47]. An upgrade to version 2021.3.11f1 (Long-Term Support, or LTS) [32] was later implemented to ensure complete compatibility with the Virtual Reality toolkit plugin (XR Interaction Toolkit version 2.0.3) (Additional file 3: Methods). For each integrated ST platform, we developed specific state-of-the-art AWs using Python executables and open-sourced tools and packages, which are

embedded within the application to function as a unified software solution (Additional file 3: Methods).

The software was developed for Windows 10 and later optimised for Windows 11 to ensure compatibility across modern systems. In addition, we also provide a macOS version that supports the full suite of Visualiser features. However, this version currently does not include the AW component, focusing instead on enabling users to access the key visualisation features seamlessly.

Features of VR-Omics

Automated Workflow

For each of the integrated ST platforms, a purpose-built AW was developed to optimise data processing and allow advanced analysis of the ST raw data. This optimisation is achieved through a user-friendly interface that enables end-to-end processing and analysis of raw data, thus eliminating the need for time-consuming data formatting steps. All proprietary data is supported as provided by the vendor, and VR-Omics automatically detects the necessary files by selecting the main directory of each sample, reducing the risk of incorrect file selection. Within the AW, users can perform a variety of operations to tailor data analysis (Additional file 2: Fig. S1), including standard filtering metrics to ensure data quality such as (i) number of counts per location, (ii) percentage of overall mitochondrial gene expression, and (iii) number of cells expressing a certain gene. These metrics can all be easily visualised across the tissue section to highlight regions of poor data quality and capture inter- or intra-tissue heterogenety (Additional file 2: Fig. S1a).

The default normalisation methods (as recommended by each analysis package) are applied, and data is log-transformed before highly variable genes (HVGs) are identified. Subsequently, principal component analysis (PCA) is performed, neighbours are computed, and UMAP or t-SNE coordinates are generated prior to performing spatially agnostic Leiden clustering or STAGATE-enhanced Leiden clustering depending on the dataset (Fig. 1e–f). The AW executes spatial analyses using various Python libraries such as Scanpy v1.9.3, SpatialDE v1.1.3, and STAGATE v1.0.1, for different commercialised and open-source ST platforms and custom data.

SVGs, crucial for understanding cell differentiation and tissue organisation, are identified using SpatialDE (1.1.3) for Visium data or Moran's *I* statistic for other data types (Additional file 2: Fig. S12a) [34].

Visualiser capabilities

Across these ST platforms, different terms are used for the smallest individual capture area of each technique, e.g., *spots*, *locus*/*loci*, *bins*, or *locations.* For consistency, we will use the term *locations* throughout the manuscript, always referring to the smallest individual capture area of the respective ST methods.

After processing their data through the AW or loading the requisite files, irrespective of the data platform used, users can explore their datasets within the Visualiser. The Visualiser offers an array of interactive features designed with input from biologists to create intuitive analysis tools and ensure availability of the right resources to address various biological questions. These features support the systematic exploration and

comparison of gene expression data across samples within a 2D desktop or VR environment (Additional file 2: Fig. S12).

Key capabilities include the visualisation of gene expression, enabling insights into the expression of significant markers, such as *EPCAM* in breast cancer, which is associated with poor prognosis [48] (Fig. 1d). This visualisation aids in correlating disease severity with tissue characteristics, further enhanced by the superimposition of metadata like clustering results or images alongside gene expression data, allowing for rapid assessment of alignment between clustering, gene expression, and tissue histology.

The top menu provides the ability to select the visualisation of clustering results, including Leiden clusters, which are run by default through the AW, or STAGATE clusters if this option was selected during AW configuration. This flexibility allows users to compare multiple clustering approaches directly within the Visualiser, enabling deeper exploration and validation of spatial patterns across the tissue. Furthermore, the user can access SVG results directly from the top menu, which displays an interactive table containing key information such as p values for each gene identified as spatially significant (Additional file 2: Fig. S12a). Genes identified as significant are also highlighted in teal within the search bar, allowing for quick identification and exploration. The SVG cut-off value can be manually adjusted by the user to apply more or less stringent filtering criteria, providing additional control over the selection of SVGs. This dynamic approach enhances the user's ability to focus on specific genes or patterns of interest, further streamlining the visualisation and interpretation of ST data.

The platform also enables the exploration of gene expression profiles, crucial for leveraging the full potential of ST data. Features like visualising two different gene expression profiles on adjacent slides or within the same tissue section, as well as vector-based gene expression differences, facilitate comparisons of markers linked to disease prognosis or aggressiveness such as *EPCAM* and *ELF3* in breast cancer [48, 49]. This comparison is valuable for understanding their impact on specific regions or cells within a tumour. Replication of actions across duplicated slides, such as ROI selection, is supported (Additional file 5: Video 3).

Gene search functionality allows users to find and visualise a gene of interest's expression through a heatmap, showcasing relative expression at each location (Fig. 1d). An alternative binary visualisation mode highlights locations with nonzero expression of the selected gene, enhancing the visibility of gene activity (Fig. 1d). Users can adjust the visualisation granularity by modifying location size or filtering out low-expression locations, applying thresholds to streamline the display (Additional file 2: Fig. S12b). If SVGs were identified using the AW, these genes are highlighted with a turquoise-colored result button for easy identification (Additional file 2: Fig. S12a).

Superimposition of other metadata, such as H&E staining or clustering results from Leiden or STAGATE calculated in the AW, is facilitated for enhanced data interpretation. When available, serial sections across a sample enable the uploading of a 3D model to improve spatial and anatomical orientation (Additional file 2: Fig. S1d), with various adjustments available to align the 3D model with the dataset.

The Visualiser's side-by-side comparison feature allows visualisation of two different gene expression profiles on adjacent slides or the same tissue section, enabling precise ROI delineation and ensuring identical analysis areas across slides (Additional file 13:

Video 4). This feature can be toggled off to merge the expressions of both genes into a normalised, vector-based difference calculation at each location, highlighting significant expression differences between the two gene profiles (Additional file 2: Fig. S1e).

Facilitating analysis of multi-slice Visium datasets

For Visium datasets, VR-Omics overcomes two common analytical challenges: (1) facilitating concatenation of multiple Visium sections taken from the same tissue in 2D for joint analysis (Fig. 1b) and (2) loading of multiple, serial sections for visualisation in 3D (Fig. 1c). The first feature is enhanced through the introduction of a visually intuitive concatenation interface. Here, each sample is represented by its histologically stained image, allowing users to rearrange slides into their original configuration via a user-friendly drag-and-drop mechanism (Additional file 4: Video 2). Additionally, slides can be effortlessly rotated, enabling precise and flexible alignment for the accurate reconstruction of original tissue sections. Following alignment, users have the capability to specify processing parameters, including the filtering of cells, genes, and mitochondrial values, as well as adjusting the sensitivity of the clustering algorithm. These inputs initiate the seamless concatenation of slides, followed by subsequent analyses and cell type clustering, streamlining the entire process for optimal data integration and interpretation.

In the second scenario, VR-Omics offers the unique option to simultaneously load multiple Visium samples if they represent serial sections of the same tissue, to visualise the tissue in 3D (Additional file 2: Fig. S1c). For this, VR-Omics provides a straightforward alignment process consisting of selecting multiple Visium sample folders that have been processed and/or analysed with the AW (Additional file 2: Fig. S1c_i). The selected datasets will be in unison, allowing the user to set the correct anatomical order from front to back of the slides. Next, all H&E images will be overlapped in a simple user interface that allows the user to rotate the slides individually, correcting misalignments of the samples on the capture areas (Additional file 2: Fig. S1c_{ii}). Furthermore, the user can set the distances between each slide in depth direction (Additional file 2: Fig. S1c_{ii}). Finally, the user can visualise the merged dataset rendered from the selected slides with the set distances and rotations as a 3D object (Additional file 2: Fig. S1c_{iii}).

The virtual reconstruction offered through VR-Omics GUI allows datasets to be interpreted by biologists in a representation that is more faithful to the whole tissue. To provide training for prospective users, the AW and Visualiser capabilities can be explored by processing of the 3D demo data of the human developing heart [24]. When dealing with 3D datasets, the user can upload a 3D model of their tissue or organ of interest and align spatial data within it. In the case of the developing human heart [24], an overlay of the 3D model provides the user a more intuitive understanding of which clusters correspond to anatomical structures within the heart, allowing for easier selection of biologically relevant ROIs across the depth of the dataset (Additional file 2: Fig. S1 d).

Expert feedback

We consulted ST experts who were first-time VR-Omics users to provide feedback assessing the effectiveness and efficiency of the end-to-end VR-Omics workflow compared to non-interactive benchmark pipelines. Experts had high spatial transcriptomics

fluency, and prior experience using analysis pipelines for the platforms Xenium (Squidpy), Visium (Seurat), and MERFISH (Squidpy). All VR-Omics analysis was performed using v3.0 of the application. A questionnaire was provided during the expert consultation to collect qualitative and quantitative feedback. All original questionnaire responses and feedback are included as Additional file 6: Questionnaire. Experts were not financially or otherwise compensated for their participation.

VR-Omics performance tests

Testing of VR-Omics processing and visualisation capabilities was conducted using VR-Omics v3.0. Tests on single slices were performed in duplicate and the mean reported. For comparison purposes, we selected a single mouse brain slide from each of the tested ST platforms. All datasets are publicly available on respective vendor websites (see Data availability). Tests were performed on a windows machine with 64 GB RAM, NVIDIA RTX A4500 graphics card, and Intel(R) Core (TM) i9-12900 K Processor 3.20 GHz. A custom python script employing psutil and GPUtil libraries was employed to measured peak GPU, CPU, and RAM usage at 0.1-s intervals.

Visium data were filtered using gene count thresholds set between 1000 and 35,000 counts, while mitochondrial reads exceeding 10% were excluded. Additionally, genes expressed in fewer than 10 locations were filtered out. In contrast, datasets from Xenium and MERFISH were processed without applying specific filter parameters (Additional file 7: Table S1). In addition to the performance tests of the AWs, a stress test of the Visualiser GUI was performed. For this test, the above mentioned Visium dataset was filtered to 2702 locations. To simulate larger datasets, we employed a modified version of VR-Omics that allowed exponential duplication of slides, creating 3D datasets by repeating the same slides. This approach enabled us to do time measurements from initiating the process until the slides were fully loaded. The dataset was scaled up incrementally to a maximum of 2048 slides, resulting in a total of 5,533,696 locations (Fig. 3c). No further interaction tests were performed after loading the data into the Visualiser. To conduct this test, the same workstation as described above was used.

Scoring ST tools using the 3D developing heart dataset

We designed a typical workflow to identify the DEGs between the right ventricle and right atrium of the heart. The workflow covers 5 steps: (1) inputting ST data; (2) clustering spots/locations; (3) assembling slices into a 3D structure; (4) manually selecting two ROIs; and (5) identifying the top DEGs between these ROIs. For each step, if the ST tool has a native feature to perform the task, we assign a score of 1. If the feature is not available natively in the ST tools, we wrote additional command-line based script (available at https://figshare.com/s/0c9d9cc265b45b5d9441) to achieve the tasks. When the DEG was performed using 3D-Cardiomics, the EdgeR [50] method was used as implemented natively in 3D-Cardiomics. When performing DEG analysis using VR-Omics and command-line based script (STitch3D, VT3D), the FindMarkers() function of Seurat v5 was used [51]. The right ventricle vs. right atrium DEG analysis was performed on the Litviňuková et al. [31] single-cell sequencing dataset also using the FindMarkers function of Seurat v5 [51] (R script available at https://figshare.com/s/0c9d9cc265b45b5d9441). These well-defined regions (right ventricle vs. right atrium) have established differences

in gene expression described in the published mammalian heart studies [30, 31] used as a chamber-specific reference marker gene set, making this dataset an optimal candidate for testing the capabilities of ST algorithms to easily identify, subset, and compare gene expression across biological ROIs.

Processing patient samples and data analyses

All samples were sequenced using the Visium FFPE Spatial Solution in conjunction with the Advanced Genomics Facility at the Walter and Eliza Hall Institute (WEHI). Samples of patient MCTHB302 were sequenced in the first batch, while the samples of MCTHB361 and of MCTHB362 were sequenced in a subsequent batch. Samples were sectioned as necessary to fit Visium capture areas (Fig. 4 and Additional file 2: Fig. S8). Outputs from both batches of Visium experiments were reanalysed through the SpaceRanger pipeline v2.0.1 [52] by the WEHI team. The outputs of the SpaceRanger pipeline for all samples were used as the inputs VR-Omics. The VR-Omics workflow included using the Visualiser to align multiple 2D slices and generated a joint, co-planar data object (Additional file 4: Video 2), and Scanpy pre-processing including clustering using STAGATE. Filter parameters were established independently for each sample. The markers for each cluster were retrieved by identifying DEGs between clusters using a Wilcoxon rank sum test within Scanpy v 1.9.6 and then filtered for an adjusted p value $\leq$ 0.05. For orthogonal validation of analysis of multi-slice datasets as individual slices, the same process was employed with an additional filter of logFC $\geq$ 0.1 for cluster markers. These markers were then used as the input for gene ontology enrichment analysis using Metascape v 3.5 [53] or, when inputs exceeded 3000 genes, Webgestalt [54]. Within Metascape, inputs were specified as belonging to *Homo sapiens*, and a standard express analysis was run. Results for the GO analysis were reported only when pathways were returned with a significant p value associated to the cluster makers used as input. When using Webgestalt, the method of interest was set as over-representation analysis and *Homo sapiens* as the organism of interest. The functional database was set to geneontology with the additional parameter of "Biological Process noRedundant," no background was chosen.

These findings were then validated orthogonally, outside of the VR-Omics framework using a series of comparable tools requiring coding experience. Samples were preprocessed and filtered in Seurat; then clustering for individual or joint objects for all patients was performed using the BayesSpace algorithm [55]. Gene ontology enrichment analysis was performed as outlined above.

Supplementary Information

The online version contains supplementary material available at https://doi.org/10.1186/s13059-025-03630-6.

Additional file 1: Video 1. Capabilities within VR-Omics for interactions with datasets using VR. Demonstrated here with Visium, 3D human developing heart dataset [24]. Ability to visualise clusters across dataset is demonstrated along with the ability to customize the visualisation of locations within a 3D dataset

Additional file 2: Supplementary figures. Collection of all supplementary figures

Additional file 3: Methods. Additional information about the input data for ST platforms, the technical specifications of VR-Omics and its corresponding AW implementation, and the features of VR-Omics is provided. Furthermore, there is additional information on the analysis of cRMs using BayesSpace [71–76]

Additional file 4: Video 2. Tutorial for loading 2D Visium data processed by VR-Omics AW into VR-Omics Visualiser for data interaction. At 0:15 s, there is a tutorial for loading 3D Visium data into VR-Omics and then perform alignment

of slides by being able to rotate and adjust each slide individually and set distances between each slide. At 0:36 s, a tutorial on how to load, easily adjust, and concatenate multiple, 2D co-planar Visium slices is available

Additional file 5: Video 3. Tutorial for loading raw datasets for processing with VR-Omics followed by examples screen in the user interface for user-defined filtering parameters and analysis options available for datasets generated with each platform

Additional file 6: Questionnaire. Collection of all expert feedback

Additional file 7: Table S1. Comparison of VR-Omics memory usage and time required for process various datasets through the AW using different filtering parameters. Datasets tested include the Xenium Human Breast Cancer FFPE dataset, the MERFISH Adult Mouse Brain Dataset, and Visium V1 human lymph node dataset

Additional file 8: Table S2. Comparison of VR-Omics time requirement for visualising multiple Visium slides

Additional file 9: Table S3. List of differentially expressed genes between the right ventricle and right atrium identified in the human embryonic heart at 6 dpc by VR-Omics [30]

Additional file 10: Table S4. List of differentially expressed genes between the right ventricle and right atrium identified in the adult human heart from the Heart Cell Atlas dataset [31]

Additional file 11: Results. Additional results for cross-platform comparisons of mouse brain slides across multiple ST platforms are available. More information on multi-slice 3D data analysis using VR-Omics and orthogonal validation of upregulated pathways in cRMs is also provided

Additional file 12: Table S5. Comparison of VR-Omics with commonly used visualisation tools for each of the ST methods supported by VR-Omics. The features described in this table show the overall capability of VR-Omics compared to the tools that are available to visualise and explore ST data

Additional file 13: Video 4. Tutorial for visualising processed datasets within VR-Omics and display of Visualiser capabilities. At 0:00 s, there is a tutorial displaying the gene search function for heatmap display of gene expression values. At 0:19 s, there is a tutorial demonstrating a binary display of gene expression across the tissue section. At 0:29 s, there is a tutorial demonstrating the ability to find regions of co-expression between two genes. At 0:48 s, a tutorial displays the capacity to duplicate a tissue section and merge expression of two gene patterns across duplicated slices. At 1:07 s, a tutorial exhibits how to select regions of interest on a duplicated slide and at 1:13 s this capability is expanded to selected the same region of interest through multiple, stacked 3D slides

Acknowledgements
We thank the patient donors and their family for the valuable samples. We thank the members of the Ramialison's, Schreiber's, Porrello's, and Elliott's lab, especially Dimitar Garkov for the technical inputs and code contribution, and Antonia Zech, Sebastian Bass-Stringer, Grzegorz Maciag and the Monash Bioinformatics Platform for helpful discussions. We thank the support of the WEHI Advanced Genomics Facility for technical advice on processing the patient samples. We thank Brett Kennedy and Patrick Marks (10x Genomics) and Jan Philipp Junker and Jeroen Bakkers for the sample data. We thank Yuen Chang and Jacquie Crawford and Francesca Bolk for support and assistance. We thank Geoff McDermott and Catherine King from 10x Genomics for their support and advice with the Visium platform. We thank Jinmiao Chen, Saskia Freytag, Sarah Williamson, Tamsin Rob and the del Monte-Nieto lab for their trialling of VR-Omics and feedback on the software.

Peer review information
Veronique van den Berghe was the primary editor of this article and managed its editorial process and peer review in collaboration with the rest of the editorial team. The peer-review history is available in the online version of this article.

Authors' contributions
Conception and design: DB, NC, ERP, DAE, KK, HTN, FS, MR. Data acquisition, analysis and interpretation: DB, NC, HC-S, DM, BC, ATP, CV, ES, SG, ERP, DAE, LW, HTN, MR. Software development: DB, NC, DW, YZ, SJ-H, JD, JS, HTN. Benchmarking: LW, NC, DB, YT, JT, HML, MD, MM, LH. Manuscript draft: DB, NC. Manuscript editing, review and intellectual feedback: all authors.

Funding
MR is funded by a Future Leader Fellowship (107328) from the Heart Foundation of Australia, a Human Frontiers Science Program Grant (RGP008/2024). MR and HTN are supported by an NHMRC Ideas Grant (APP1180905). NC is supported a 10x-Millenium Science's Spatial Pioneer fellowship. F.J.R is supported by NHMRC Ideas Grants (APP2036469, APP2019853). Additional infrastructure funding to the Murdoch Children's Research Institute was provided by the Australian Government National Health and Medical Research Council Independent Research Institute Infrastructure Support Scheme. The Australian Regenerative Medicine Institute is supported by grants from the State Government of Victoria and the Australian Government. The Novo Nordisk Foundation Center for Stem Cell Medicine is supported by Novo Nordisk Foundation grants (NNF21CC0073729). FS, SJH, and KK are supported by the Deutsche Forschungsgemeinschaft (DFG) under Germany's Excellence Strategy--EXC 2117--422037984, and DFG project ID 251654672--TRR 161.

Data availability
VR-Omics software
VR-Omics (licensed under the OSI-compliant MIT license) can be downloaded directly via the following links:
• Figshare (Windows, DOI: https://doi.org/10.6084/m9.figshare.28259834.v3): https://widgets.figshare.com/articles/28259834/embed?show_title=1 [56]
• Figshare (MacOs – Beta Version; DOI: https://doi.org/10.6084/m9.figshare.28340495.v4): https://figshare.com/articles/software/VR-Omics_MAC/28340495?file=52114634 [57]

• Source code (Unity Engine required) is publicly available at <https://github.com/Ramialison-Lab/VR-Omics> [58]
The VR-Omics software, including tutorials and demos, is also available at: https://ramialison-lab.github.io/pages/vromics.html [59]
GitHub source code (licensed under the OSI-compliant MIT license): https://doi.org/10.5281/zenodo.15227021
Rhabdomyoma samples and third party datasets
The paediatric cardiac rhabdomyomas Visium profiling data have been deposited in NCBI GEO under accession number GSE252228 [60]. Third-party datasets used in this study are available under EGAS accession EGAS00001003996 [24]. Data for cross-platform comparison can be accessed via Figshare at <https://figshare.com/s/78bcc6320cf3b2ee64af> [61].
VR-Omics performance tests and comparison
Custom R scripts for visualising Stitch3D data and performing differential gene expression analysis on datasets by Asp et al. 2019 [24] and Litviňukova et al. 2021 [31] are available on Figshare at <https://figshare.com/s/0c9d9cc265b45b5d9441> [62].
The datasets used for performance testing can be accessed at the following links:
• Visium: https://cf.10xgenomics.com/samples/spatial-exp/1.1.0/V1_Adult_Mouse_Brain/V1_Adult_Mouse_Brain_web_summary.html [63]
• Xenium (Mouse Brain Replicate 1): https://cf.10xgenomics.com/samples/xenium/1.0.2/Xenium_V1_FF_Mouse_Brain_MultiSection_1/Xenium_V1_FF_Mouse_Brain_MultiSection_1_analysis_summary.html [64]
• Stereo-seq: https://db.cngb.org/stomics/datasets/STDS0000234/summary [65] -
• MERFISH (Vizgen): Available via the Vizgen Data Release Program: https://info.vizgen.com/mouse-brain-data [66]
Additionally, the following public datasets were used for the validation of VR-Omics throughout the manuscript:
• Visium Human Lymph Node V1 dataset: <https://www.10xgenomics.com/datasets/human-lymph-node-1-standard-1-0-0> [67]
• Xenium Human Breast Cancer FFPE dataset: https://www.10xgenomics.com/products/xenium-in-situ/preview-dataset-human-breast [68]
• MERFISH Mouse Brain Receptor dataset: https://info.vizgen.com/mouse-brain-data [69]
• Visium Multi-Slice Adult Mouse Brain Coronal dataset: https://www.10xgenomics.com/datasets/mouse-brain-section-coronal-1-standard [70].

Declarations

Ethics approval and consent to participate
Human ethics for cardiac tissue biobanking and human pluripotent stem cell research was approved by The Royal Children's Hospital Melbourne Human Research Ethics Committee (approval numbers: HREC 38192). Informed consent was obtained from all human participants, and studies were conducted in accordance with the approved protocols and guidelines from the National Health and Medical Research Council of Australia.

Consent for publication
Not applicable.

Competing interests
Consent for publication of de-identified data was obtained from all participants included in this publication.

Author details
[1]Novo Nordisk Foundation Center for Stem Cell Medicine, Murdoch Children's Research Institute, Parkville, VIC 3052, Australia. [2]Department of Paediatrics, Faculty of Medicine, Dentistry & Health Sciences, University of Melbourne, Melbourne 3010, Australia. [3]Department of Computer and Information Science, University of Konstanz, Constance 78464, Germany. [4]Anatomical Pathology, The Royal Children's Hospital, Melbourne, VIC 3052, Australia. [5]Melbourne Centre for Cardiovascular Genomics and Regenerative Medicine, The Royal Children's Hospital, Melbourne, VIC 3052, Australia. [6]Department of Anatomy and Physiology, University of Melbourne, Parkville, VIC 3052, Australia. [7]Collaborative Centre for Genomic Cancer Medicine, University of Melbourne, Melbourne, Victoria, Australia. [8]Department of Clinical Pathology, University of Melbourne, Melbourne, Victoria, Australia. [9]Department of Anatomy and Developmental Biology, Monash Biomedicine Discovery Institute, Monash University, Melbourne, VIC 3800, Australia. [10]Adelaide Centre for Epigenetics, Faculty of Medicine and Health Sciences, The University of Adelaide, Adelaide, South Australia 5000, Australia. [11]South Australian immunoGENomics Cancer Institute, Faculty of Medicine and Health Sciences, The University of Adelaide, Adelaide, South Australia 5000, Australia. [12]Department of Clinical Pathology, University of Melbourne, Melbourne, VIC, Australia. [13]Australian Regenerative Medicine Institute, System Biology Institute, Monash University, Clayton, Melbourne, VIC 3168, Australia. [14]Faculty of Information Technologies, Monash University, Melbourne, VIC 3168, Australia.

Received: 30 May 2024 Accepted: 23 May 2025
Published online: 02 July 2025

References

1. Marx V. Method of the year: spatially resolved transcriptomics. Nat Methods. 2021;18:9–14.
2. Cheng M, Jiang Y, Xu J, Mentis AA, Wang S, Zheng H, Sahu SK, Liu L, Xu X. Spatially resolved transcriptomics: a comprehensive review of their technological advances, applications, and challenges. J Genet Genomics. 2023;50:625–40.
3. Waylen LN, Nim HT, Martelotto LG et al. From wholemount to single-cell spatial assessment of gene expression in 3D. Commun Biol. 2020;3:602. https://doi.org/10.1038/s42003-020-01341-1.

4. Berglund E, Maaskola J, Schultz N, Friedrich S, Marklund M, Bergenstråhle J, Tarish F, Tanoglidi A, Vickovic S, Larsson L, et al. Spatial maps of prostate cancer transcriptomes reveal an unexplored landscape of heterogeneity. Nat Commun. 2018;9:2419.
5. Chen A, Liao S, Cheng M, Ma K, Wu L, Lai Y, Qiu X, Yang J, Xu J, Hao S, et al. Spatiotemporal transcriptomic atlas of mouse organogenesis using DNA nanoball-patterned arrays. Cell. 2022;185:1777-1792.e1721.
6. Wang G, Zhao J, Yan Y, Wang Y, Wu AR, Yang C. Construction of a 3D whole organism spatial atlas by joint modelling of multiple slices with deep neural networks. Nat Mach Intell. 2023;5:1200–13.
7. Guo L, Li Y, Qi Y, Huang Z, Han K, Liu X, Liu X, Xu M, Fan G. VT3D: a visualization toolbox for 3D transcriptomic data. J Genet Genomics. 2023;50:713–9.
8. Fan Z, Chen R, Chen X. SpatialDB: a database for spatially resolved transcriptomes. Nucleic Acids Res. 2020;48:D233–7.
9. Xu Z, Wang W, Yang T, Li L, Ma X, Chen J, Wang J, Huang Y, Gould J, Lu H, et al. STOmicsDB: a comprehensive database for spatial transcriptomics data sharing, analysis and visualization. Nucleic Acids Res. 2023;52:D1053–61.
10. Yuan Z, Pan W, Zhao X, Zhao F, Xu Z, Li X, Zhao Y, Zhang MQ, Yao J. SODB facilitates comprehensive exploration of spatial omics data. Nat Methods. 2023;20:387–99.
11. Li Y, Dennis S, Hutch MR, Li Y, Broad MS, Zeng Z, Luo Y. SOAR: a spatial transcriptomics analysis resource to model spatial variability and cell type interactions. Biorxiv 2022:2022.2004.2017.488596. https://doi.org/10.1101/2022.04.17.488596.
12. Bienroth D, Nim HT, Garkov D, Klein K, Jaeger-Honz S, Ramialison M, Schreiber F. Spatially resolved transcriptomics in immersive environments. Visual Computing for Industry, Biomedicine, and Art. 2022;5:1–13.
13. Ma S, Fang X, Yao Y, Li J, Morgan DC, Xia Y, Kwok CSM, Lo MCK, Siu DMD, Tsia KK, et al. StarmapVis: an interactive and narrative visualisation tool for single-cell and spatial data. Comput Struct Biotechnol J. 2023;21:1598–605.
14. Yang A, Yao Y, Li J, Ho JWK. Starmap: immersive visualisation of single cell data using smartphone-enabled virtual reality. Biorxiv. 2018:324855. https://doi.org/10.1101/324855.
15. Xenium FFPE human breast with custom add-on panel [https://www.10xgenomics.com/datasets/xenium-ffpe-human-breast-with-custom-add-on-panel-1-standard] (2023)
16. Bondavalli D, White SM, Steer A, Pflaumer A, Winship I. Is cardiac rhabdomyoma a feature of Birt Hogg Dubé syndrome?. Am J Med Genet A. 2015;167a:802–4.
17. Holley DG, Martin GR, Brenner JI, Fyfe DA, Huhta JC, Kleinman CS, Ritter SB, Silverman NH. Diagnosis and management of fetal cardiac tumors: a multicenter experience and review of published reports. J Am Coll Cardiol. 1995;26:516–20.
18. Berger JT, Holubkov R, Reeder R, Wessel DL, Meert K, Berg RA, Bell MJ, Tamburro R, Dean JM, Pollack MM. Morbidity and mortality prediction in pediatric heart surgery: physiological profiles and surgical complexity. J Thorac Cardiovasc Surg. 2017;154:620-628.e626.
19. Joshi M, Kumar S, Noshirwani A, Harky A. The current management of cardiac tumours: a comprehensive literature review. Braz J Cardiovasc Surg. 2020;35:770–80.
20. Irabor B, Khan A, Noga M, Myers K, Greenway SC, Hassanabad AF. Arrhythmia as a presenting feature of atypical cardiac rhabdomyoma in children. CJC Pediatr Congenit Heart Dis. 2024;3:125-8.
21. Cai Z, Thomas J, Alava I, Aakash N, Saluja K, Zhu H. Fetal type rhabdomyoma of the soft palate in an adult patient: report of one case and review of the literature. Head Neck Pathol. 2019;13:182–7.
22. Kotulska K, Larysz-Brysz M, Grajkowska W, Jóźwiak J, Włodarski P, Sahin M, Lewin-Kowalik J, Domańska-Pakieła D, Jóźwiak S. Cardiac rhabdomyomas in tuberous sclerosis complex show apoptosis regulation and mTOR pathway abnormalities. Pediatr Dev Pathol. 2009;12:89–95.
23. Zou Z, Tao T, Li H, Zhu X. mTOR signaling pathway and mTOR inhibitors in cancer: progress and challenges. Cell Biosci. 2020;10:31.
24. Asp M, Giacomello S, Larsson L, Nilsson M, Lundeberg J. A spatiotemporal organ-wide gene expression and cell atlas of the developing human heart. Cell. 2019;179:1647-1660.e1619.
25. Loupe Browser - 10x Genomics [https://www.10xgenomics.com/products/loupe-browser]
26. What is Loupe Browser? - software - single cell gene expression - official 10x Genomics support [https://support.10xgenomics.com/single-cell-gene-expression/software/visualization/latest/what-is-loupe-cell-browser]
27. Xenium Explorer - official 10x Genomics support [https://www.10xgenomics.com/support/software/xenium-explorer]
28. MERSCOPE spatial transcriptomics | Vizgen [https://vizgen.com/products/]
29. Stereopy - spatial transcriptomics analysis in Python — stereopy v0.1 documentation [https://stereopy.readthedocs.io/en/latest/]
30. Mohenska M, Tan NM, Tokolyi A, Furtado MB, Costa MW, Perry AJ, Hatwell-Humble J, van Duijvenboden K, Nim HT, Ji YMM, et al. 3D-cardiomics: a spatial transcriptional atlas of the mammalian heart. JMCC. 2022;163:20–32.
31. Litviňuková M, Talavera-López C, Maatz H, Reichart D, Worth CL, Lindberg EL, Kanda M, Polanski K, Heinig M, Lee M, et al. Cells of the adult human heart. Nature. 2020;588:466–72.
32. Unity Game Engine, version 2021.3.11f1 [https://unity.com]
33. Dong K, Zhang S. Deciphering spatial domains from spatially resolved transcriptomics with an adaptive graph attention auto-encoder. Nat Commun. 2022;13:1739.
34. Svensson V, Teichmann SA, Stegle O. SpatialDE: identification of spatially variable genes. Nat Methods. 2018;15:343–6.
35. Du MRM, Wang C, Law CW, Amann-Zalcenstein D, Anttila CJA, Ling L, Hickey PF, Sargeant CJ, Chen Y, Ioannidis LJ, et al: Spotlight on 10x Visium: a multi-sample protocol comparison of spatial technologies. bioRxiv. 2024:2024.2003.2013.584910.

36. Clausen L, Stein A, Grønbæk-Thygesen M, Nygaard L, Søltoft CL, Nielsen SV, Lisby M, Ravid T, Lindorff-Larsen K, Hartmann-Petersen R. Folliculin variants linked to Birt-Hogg-Dubé syndrome are targeted for proteasomal degradation. PLoS Genet. 2020;16: e1009187.
37. Hasumi Y, Baba M, Hasumi H, Huang Y, Lang M, Reindorf R, Oh H-B, Sciarretta S, Nagashima K, Haines DC, et al. Folliculin (Flcn) inactivation leads to murine cardiac hypertrophy through mTORC1 deregulation. Hum Mol Genet. 2014;23:5706–19.
38. Hasumi H, Baba M, Hong S-B, Hasumi Y, Huang Y, Yao M, Valera VA, Linehan WM, Schmidt LS. Identification and characterization of a novel folliculin-interacting protein FNIP2. Gene. 2008;415:60–7.
39. Siggs OM, Stockenhuber A, Deobagkar-Lele M, Bull KR, Crockford TL, Kingston BL, Crawford G, Anzilotti C, Steeples V, Ghaffari S, et al. Mutation of Fnip1 is associated with B-cell deficiency, cardiomyopathy, and elevated AMPK activity. Proc Natl Acad Sci. 2016;113:E3706–15.
40. Uxa S, Castillo-Binder P, Kohler R, Stangner K, Müller GA, Engeland K. Ki-67 gene expression. Cell Death Differ. 2021;28:3357–70.
41. Zhou B, Caudal A, Tang X, Chavez JD, McMillen TS, Keller A, Villet O, Zhao M, Liu Y, Ritterhoff J, et al. Upregulation of mitochondrial ATPase inhibitory factor 1 (ATPIF1) mediates increased glycolysis in mouse hearts. J Clin Invest. 2022;132:e155333.
42. King MS, Thompson K, Hopton S, He L, Kunji ERS, Taylor RW, Ortiz-Gonzalez XR. Expanding the phenotype of de novo SLC25A4-linked mitochondrial disease to include mild myopathy. Neurology Genetics. 2018;4: e256.
43. Hasumi Y, Baba M, Hasumi H, Huang Y, Lang M, Reindorf R, Oh Hb, Sciarretta S, Nagashima K, Haines DC, et al. Folliculin (Flcn) inactivation leads to murine cardiac hypertrophy through mTORC1 deregulation. Hum Mol Genet. 2014;23:5706–19.
44. Lin Y, Yang JYH. 3D reconstruction of spatial expression. Nat Methods. 2022;19:526–7.
45. Schott M, León-Periñán D, Splendiani E, Strenger L, Licha JR, Pentimalli TM, Schallenberg S, Alles J, Samut Tagliaferro S, Boltengagen A, et al. Open-ST: high-resolution spatial transcriptomics in 3D. Cell. 2024;187:3953-3972.e3926.
46. Du J, Yang YC, An ZJ, Zhang MH, Fu XH, Huang ZF, Yuan Y, Hou J. Advances in spatial transcriptomics and related data analysis strategies. J Transl Med. 2023;21:330.
47. Unity Game Engine, Version 2019.4.26f1 [https://unity.com]
48. Soysal SD, Muenst S, Barbie T, Fleming T, Gao F, Spizzo G, Oertli D, Viehl CT, Obermann EC, Gillanders WE. EpCAM expression varies significantly and is differentially associated with prognosis in the luminal B HER2(+), basal-like, and HER2 intrinsic subtypes of breast cancer. Br J Cancer. 2013;108:1480–7.
49. Zhang Z, Zhang J, Li J, Geng H, Zhou B, Zhang B, Chen H. miR-320/ELF3 axis inhibits the progression of breast cancer via the PI3K/AKT pathway. Oncol Lett. 2020;19:3239–48.
50. Robinson MD, McCarthy DJ, Smyth GK. edgeR: a Bioconductor package for differential expression analysis of digital gene expression data. Bioinformatics. 2010;26:139–40.
51. Hao Y, Stuart T, Kowalski MH, Choudhary S, Hoffman P, Hartman A, Srivastava A, Molla G, Madad S, Fernandez-Granda C, Satija R. Dictionary learning for integrative, multimodal and scalable single-cell analysis. Nat Biotechnol. 2024;42:293–304.
52. What is Space Ranger? - software - spatial gene expression - official 10x Genomics support [https://support.10xgenomics.com/spatial-gene-expression/software/pipelines/latest/what-is-space-ranger]
53. Zhou Y, Zhou B, Pache L, Chang M, Khodabakhshi AH, Tanaseichuk O, Benner C, Chanda SK. Metascape provides a biologist-oriented resource for the analysis of systems-level datasets. Nat Commun. 2019;10:1–10.
54. Liao Y, Wang J, Jaehnig EJ, Shi Z, Zhang B. WebGestalt 2019: gene set analysis toolkit with revamped UIs and APIs. Nucleic Acids Res. 2019;47:W199–205.
55. Zhao E, Stone MR, Ren X, Guenthoer J, Smythe KS, Pulliam T, Williams SR, Uytingco CR, Taylor SEB, Nghiem P, et al. Spatial transcriptomics at subspot resolution with BayesSpace. Nat Biotechnol. 2021;39:1375–84.
56. Bienroth D, Charitakis N, Ding J, Zhang Y, Nim HT, Ramialison M, et al. VR-Omics (Windows v3.0): automated integration of multi-slice spatial transcriptomics data in 2D and 3D. Figshare. 2025. https://doi.org/10.6084/m9.figshare.28259834.v3.
57. Bienroth D, Charitakis N, Ding J, Zhang Y, Nim HT, Ramialison M, et al: VR-Omics (MAC): automated integration of multi-slice spatial transcriptomics data in 2D and 3D. Figshare. [https://doi.org/10.6084/m9.figshare.28340495.v4] (2025)
58. Bienroth D, Charitakis N, Ding J, Zhang Y, Nim HT, Ramialison M, et al: VR-Omics (source code): automated integration of multi-slice spatial transcriptomics data in 2D and 3D. GitHub. [https://github.com/Ramialison-Lab/vr-omics] (2025)
59. Bienroth D, Charitakis N, Ding J, Zhang Y, Nim HT, Ramialison M, et al: VR-Omics (documentation): automated integration of multi-slice spatial transcriptomics data in 2D and 3D. Github. [https://ramialison-lab.github.io/pages/vromics.html] (2025)
60. Bienroth D, Charitakis N, Ding J, Zhang Y, Nim HT, Ramialison M, et al: Spatially resolved transcriptomics exploration in 3D desktop and virtual reality environments with VR-Omics. GSE252228. Gene Expression Omnibus [https://www.ncbi.nlm.nih.gov/geo/query/acc.cgi?acc=GSE252228] (2025)
61. Bienroth D, Charitakis N, Ding J, Zhang Y, Nim HT, Ramialison M, et al: Sample datasets for VR-Omics cross platform comparison. Figshare. [https://figshare.com/s/78bcc6320cf3b2ee64af] (2025)
62. Bienroth D, Charitakis N, Ding J, Zhang Y, Nim HT, Ramialison M, et al: VR-Omics - additional resources. Figshare. [https://figshare.com/s/0c9d9cc265b45b5d9441] (2025)
63. V1_Adult_Mouse_Brain - adult mouse brain (coronal) [https://cf.10xgenomics.com/samples/spatial-exp/1.1.0/V1_Adult_Mouse_Brain/V1_Adult_Mouse_Brain_web_summary.html]
64. Xenium (mouse brain replicate 1) [https://cf.10xgenomics.com/samples/xenium/1.0.2/Xenium_V1_FF_Mouse_Brain_MultiSection_1/Xenium_V1_FF_Mouse_Brain_MultiSection_1_analysis_summary.html]
65. SAW: an efficient and accurate data analysis workflow for Stereo-seq spatial transcriptomics (dataset ID: STDS0000234) [https://db.cngb.org/stomics/datasets/STDS0000234/summary] (2023)

66. Vizgen MERFISH mouse brain receptor map [https://info.vizgen.com/mouse-brain-data] (2022)
67. Human lymph node [https://www.10xgenomics.com/datasets/human-lymph-node-1-standard-1-0-0] (2019)
68. Human breast cancer (block A section 1) - 10x Genomics [https://www.10xgenomics.com/resources/datasets/human-breast-cancer-block-a-section-1-1-standard-1-0-0] (2019)
69. Vizgen MERFISH mouse receptor map - Vizgen data release V1.0. [https://info.vizgen.com/mouse-brain-map?submissionGuid=327847ae-b16b-4418-bee2-14ca53e869a2] (2022)
70. Mouse brain section (coronal) [https://www.10xgenomics.com/datasets/mouse-brain-section-coronal-1-standard] (2022)
71. Law CW, Chen Y, Shi W, Smyth GK. voom: precision weights unlock linear model analysis tools for RNA-seq read counts. Genome Biol. 2014;15:R29.
72. Murdoch D, Adler D. rgl: 3D Visualization Using OpenGL. 2025. https://github.com/dmurdoch/rgl.
73. Satija R, Farrell JA, Gennert D, Schier AF, Regev A. Spatial reconstruction of single-cell gene expression data. 2015;33:495–502.
74. BGI: SAW: Stereo-seq analysis workflow [https://github.com/STOmics/SAW] (2021)
75. King MS, Thompson K, Hopton S, He L, Kunji ERS, Taylor RW, Ortiz-Gonzalez XR. Expanding the phenotype of de novo SLC25A4-linked mitochondrial disease to include mild myopathy. Neurol Genet. 2018;4: e256.
76. A spatiotemporal organ-wide gene expression and cell atlas of the developing human heart. EGAS00001003996. European Genome-Phenome Archive. https://ega-archive.org/studies/EGAS00001003996 (2019)

Publisher's Note